Aachen Institute for Advanced Study in Computational Engineering Science

Preprint: AICES-2008-8

26/November/2008

A Literature Review of the Extended Finite Element Method with Emphasis on Higher Order Approximations

K. W. Cheng and T. P. Fries

RWTH AACHEN UNIVERSITY

AICES

Financial support from the Deutsche Forschungsgemeinschaft (German Research Association) through grant GSC 111 is gratefully acknowledged.

List of AICES technical reports: http://www.aices.rwth-aachen.de/preprints

A Literature Review of the Extended Finite Element Method with Emphasis on Higher Order Approximations

Kwok Wah Cheng, Thomas-Peter Fries

November 25, 2008

Abstract

The Extended Finite Element Method (XFEM) is a numerical method for modelling arbitrary discontinuities in finite elements by extending the piecewise polynomial approximation space of the standard FEM to include discontinuous function spaces in local regions of the computational domain via a partition-of-unity concept. This report gives a basic introduction to the fundamentals of the XFEM and reviews its current state of development with particular emphasis on its application to two-fluid flows. Particular attention has also been devoted to the systematic development of the XFEM as an offspring of the Partition-of-Unity Method (PUM).

Contents

1 Introduction

Many physical phenomena in engineering and science can be described in terms of partial differential equations. In general, solving these equations by classical analytical methods for arbitrary geometries is almost impossible. The finite element method (FEM) is a numerical approach by which these partial differential equations can be approximated. The basic idea of FEM is to divide the body into finite elements connected by nodes, such that the element edges are aligned with the geometry of the problem. As such, even problems with complicated geometries can be adequately modelled by a skillful manipulation of the finite element mesh, see Fig. 1.

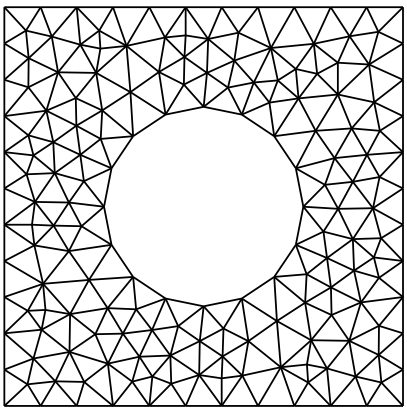

Figure 1: FEM mesh for a problem with "complicated" geometry.

For physical problems which admit smooth solutions, the piecewise continuous polynomial function space of the standard finite element method is usually sufficient to yield accurate results. However, for problems whose solutions exhibit kinks, jumps, singularities or other special solution characteristics, the standard finite element approximation requires considerable mesh refinement to resolve such features if the elements edges are not aligned with the discontinuties. Further, if the discontinuity evolves with time, the nodes and elements must be updated (remeshed) continuously. For multiple discontinuities and three dimensional problems, this becomes rapidly intractable. Therefore, the development of a method for modelling arbitrary discontinuities in finite elements on a fixed mesh without remeshing is desirable.

The above paragraphs provide the impetus and motivation for the development of a new class of computational methods called *enriched* finite element methods which yield accurate results and yet do not require the mesh to conform to discontinuities in the approximating function or its derivatives (see Fig. 2). They also avoid remeshing for moving discontinuities. This is accomplished by extending the finite element approximation space to be able to reproduce specific enrichment functions that are representative of these discontinuous features. Enriched methods have been concurrently developed by two research groups; in one, they are called the Extended Finite Element Method (XFEM) [48, 27, 14] and in the other, they are referred to as the Generalized Finite Element Method (GFEM) [60, 61, 62]. Both methods rely on the partition of unity (PUM) approach introduced by Melenk and Babuška [9] and Duarte and Oden [28]. The XFEM is also known as a *local* PUM approach since the enrichment is localized to the vicinity of the discontinuity in order to reduce the number of unknowns and improve the conditioning of the system of equations.

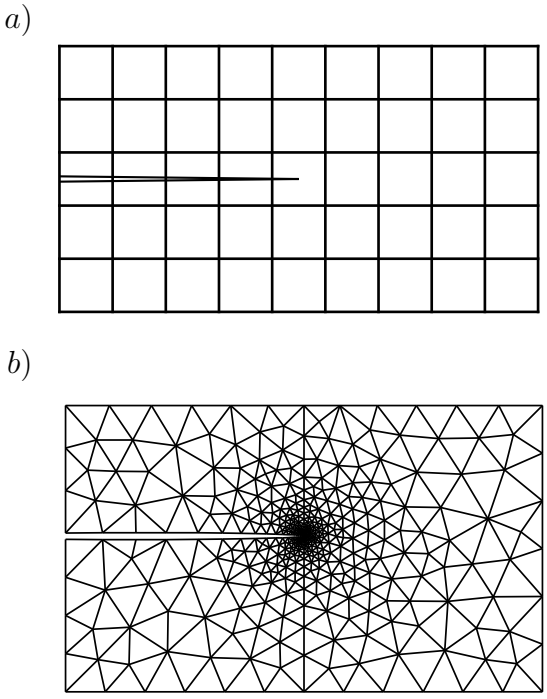

Figure 2: Comparison of meshes for an edge crack used in a) the XFEM, and b) the standard FEM.

While the XFEM has been mainly applied to time-independent crack problems (see e.g.

[48, 25, 64, 42]), there is also a huge potential of the XFEM in modelling time-dependent problems where constant remeshing is needed for the standard FEM approximation. Recent applications of XFEM to time-dependent problems include Belytschko *et al.* [13] who consider dynamic crack growth using a cohesive law, dynamic solidification problems in Chessa *et al.* [22], Dolbow *et al.* [26], Ji *et al.* [41] and two phase incompressible flow problems in Chessa and Belytschko [19, 18] and Fries [30].

The numerical simulation of two-fluid flows has a long tradition and remains an active field of research, see e.g. [35, 70, 39, 38, 65, 67]. In incompressible two-fluid flows, the velocity and pressure fields and/or their gradients are discontinuous along the interfaces between the fluids. As the interface evolves with time and cuts through the elements, the standard finite element approximation performs poorly unless constant remeshing is carried out such that the element edges are aligned with the interface throughout the simulation. The XFEM, on the other hand, ensures high accuracy even if the discontinuities lie within the elements, due to the enriched approximation space which is able to reproduce the discontinuous features within the elements. This allows for the convenient use of a fixed mesh throughout the simulation.

The interface between the two fluids is usually described by either of two classes of methods: (a) the interface-tracking methods which employ an explicit tracking of the interface with a deforming mesh which conforms to the interface, and (b) the interface-capturing methods which employ an implicit capturing of the interface using a fixed grid. Due to the deforming mesh used in the interface-tracking methods, they are only suited for problems with small interfacial displacements and no topological changes. On the other hand, large interfacial displacements and existence of topological changes do not pose a problem for the interface-capturing methods. In this project, an interface-capturing method, the level-set method, is coupled with the XFEM to solve two-fluid flow problems with the aim of achieving a higher-order convergence of the solution. The level-set method is an excellent complement to the XFEM as both require only a fixed mesh to be used throughout the simulation and the level-set function can also be used to construct enrichment functions within the XFEM framework.

This report is organized as follows: The level-set method is first introduced in section 2. The representation of interfaces by implicit functions and its advantages are given. Also, various related issues such as localization, interpolation and reinitialization are discussed. This is then followed by an introduction to the XFEM in section 3. There, a chronological overview of the XFEM is first given. Then, a description of the development of the XFEM

formulation is given with particular emphasis on the method as a special case of the Partition-of-Unity method (PUM). In section 3.3, problems in blending elements in the standard XFEM are described along with various proposed solutions. In particular, it is emphasized how such problems can be eliminated from the outset if admissible localized global enrichment functions are first chosen – an idea which arises naturally within the original PUM framework. In section 3.4, the derivation of the weak form from the classical strong form is demonstrated for the Laplace equation with discontinuous coefficients. A description of the application of the XFEM to cracks is given in section 3.5. A list of various other XFEM applications is also given in the form of a table in this section. In section 3.6, an account of the quest for achieving higher accuracy and higher rates of convergence in XFEM applied to cracks is given. This section also demonstrates how a hybrid XFEM-Global-Local method can be realized if the discontinuity is exactly spanned by the enrichment functions alone (without the need for additional PU functions). In section 4, the expression for the surface tension on an interface is derived and the governing equations of two-fluid flows are given. In section 4.3, the basic ideas of a space-time formulation are given. The report ends with a conclusion in section 5.

2 The Level-Set Method

2.1 Description of Discontinuous Interfaces

Many physical phenomena are formulated in terms of integral equations derived by considering the physical system as a whole. Such integral statements hold across discontinuous interfaces within the system. Away from these discontinuities where the field variables are smooth, these integral equations can be well approximated by partial differential equations (PDEs) based on the continuum hypothesis. Many numerical approximations of physical problems are based on discrete approximations to these PDEs. It should be noted that these numerical approximations fail to represent the physical picture at or near the discontinuities since the continuum hypothesis is violated in such regions. We are now confronted with two approaches to tackle this problem. The first is to circumvent the problem by adding artificial dissipation to smear out the discontinuous interface and solving this modified, smooth problem, see e.g. [52]. The second is to treat the discontinuity as an internal boundary and impose appropriate jump conditions across this boundary. The first approach, though easy to implement, may lead to unrealistic approximations of certain

properties at the physical interface. For example, in two-fluid flow problems, this approach leads to loss of all surface-tension effects [15]. The second approach entails tracking of the interface location as it evolves with time. For this second approach, two classes of methods exist: (a) the interface tracking methods, and (b) the interface capturing methods.

The interface-tracking methods employ an explicit tracking of the interface via a *Lagrangian* formulation. Suppose the velocity, $\boldsymbol{u}(\boldsymbol{x})$ of each point $\boldsymbol{x}$ on the interface is known and we wish to move all points on the interface with this velocity field, the Lagrangian formulation would entail solving the ordinary differential equation

$$\frac{\mathrm{d}\boldsymbol{x}}{\mathrm{d}t} = \boldsymbol{u}(\boldsymbol{x}) \tag{2.1}$$

for every point $\boldsymbol{x}$ on the interface. In a discrete setting, the moving front is initially discretized into a finite number of elements which follow the interface throughout the simulation. The results are satisfactory provided the connectivity does not change (i.e. no merging or pinching apart of the interface) and the interface elements are not distorted too much. However, results can deteriorate rapidly if one does not periodically regularize the deforming elements to maintain a reasonable aspect ratio of the elements, see Fig. 3. Examples of interface tracking methods include the front tracking method [72] and the Arbitrary Eulerian-Lagrangian (ALE) method [39].

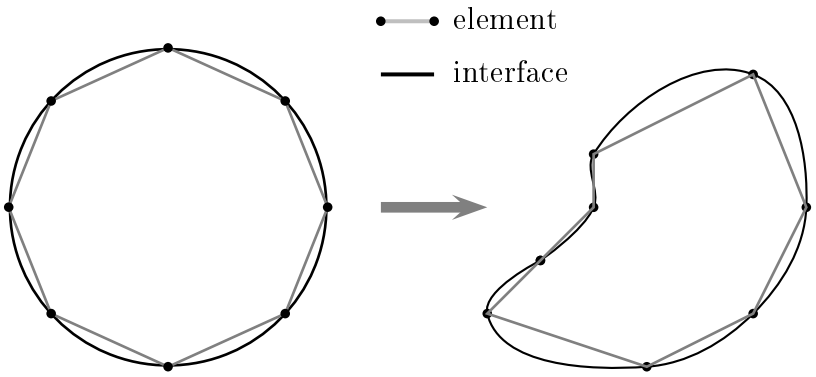

Figure 3: Distortion of one-dimensional elements in a Lagrangian formulation.

The interface-capturing methods involve an implicit description of the interface. One of the earliest methods employed is the marker and cell method (MAC) of Harlow and Welch [36].

Marker particles are scattered initially to identify each material region in the computational domain. These particles are then transported in a Lagrangian manner along with the materials. The interface is then reconstructed using the marker particle densities in the mixed cells (cells with marker particles of two or more materials). The main disadvantage of the MAC method is that many marker particles are needed per computational cell to get a well-defined interface. Another method, the volume of fluid method (VOF) [38], is proposed to overcome this deficiency. The VOF method is a fractional marker volume method which defines the interface by computing the fractional volume of each material occupied in each computational cell. These fractional volumes range from 0.0 (no marker material) to 1.0 (completely filled with the marker material), see Fig. 4. A few other interface-capturing methods exist. Of particular interest in this study is the level-set method [50] which will be described in the next section.

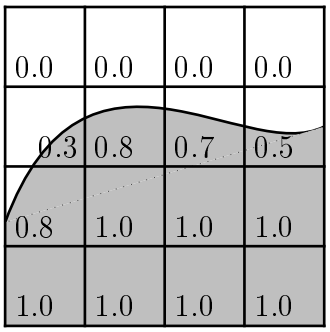

Figure 4: Volume of fluid method where numbers displayed in each cell represent the associated volume fractions of the marker material.

2.2 Representation of Interfaces by Implicit Functions

In this section, we introduce the level-set method as a method for implicit representation of interfaces. An implicit interface representaion defines the interface as the isocontour of some implicit function (called the level-set function). We note that the space on which the isocontour is defined is one dimension lower than that of the level-set function. More generally, if the level-set function $\phi(\boldsymbol{x})$ is a surface defined on all $\boldsymbol{x} \in \mathbf{R}^n$, its isocontour

will then be defined on the $\mathbf{R}^{n-1}$ space. For example, suppose our level-set function is defined by

$$\phi(\boldsymbol{x}) = |\boldsymbol{x}|^2 - c, \qquad \forall \boldsymbol{x} \in \mathbf{R}^2, \tag{2.2}$$

the equation of the isocontour represented by $\phi(\boldsymbol{x}) = 0$ will then be given by:

$$y = \sqrt{c - x^2}, \qquad \forall x \in [-\sqrt{c}, \sqrt{c}], \;\; c \in \mathbf{R}^+ \tag{2.3}$$

which is a circle with radius $\sqrt{c}$, centered at the origin of the $\mathbf{R}^2$ plane. The level-set function is illustrated in Fig. 5. We note that the circle is defined on $[-\sqrt{c}, \sqrt{c}]$ which is one dimension lower than the $\mathbf{R}^2$ space on which the level-set function $\phi(\boldsymbol{x})$ is defined. Also, it is not necessary to use the $\phi(\boldsymbol{x}) = 0$ isocontour to represent the interface. For example, to represent the *same* circle in (2.3) using the $\phi(\boldsymbol{x}) = d$ isocontour, we can employ $\phi_d(\boldsymbol{x}) = \phi(\boldsymbol{x}) + d$ as the level-set function.

Such a representation of the interface might at first seem wasteful since the level-set function is a surface defined for all $\boldsymbol{x} \in \mathbf{R}^2$ whereas the interface is only a circle with dimension $\mathbf{R}^1$. There are, however, several advantages associated with this *higher dimensional* representation of the interface. For example, the implicit representation can handle dynamic interfaces which exhibit topological changes (pinching apart of the interface or merging of several pieces of the interface) with ease whereas the Lagrangian mesh in an explicit representation has to be resolved over and over again every time pieces of the surface merge together or pinch apart. For the implicit representation, connectivity does not need special treatment and a uniform Cartesian grid can be used with straightforward generalization of the technique from $\mathbf{R}^2$ to $\mathbf{R}^3$.

We shall now derive the level-set equation with respect to the same example introduced earlier. We note that the level-set function in (2.2) divides the entire $\mathbf{R}^2$ space into two distinct regions, $\Omega^-(t)$ and $\Omega^+(t)$ which along with the interface $\Gamma(t)$, are subject to the following conditions:

$$\phi(\boldsymbol{x}, t) \begin{cases} < 0 & \text{in } \Omega^-(t) \\ = 0 & \text{on } \Gamma(t) \\ > 0 & \text{in } \Omega^+(t), \end{cases} \tag{2.4}$$

where $\boldsymbol{x} \in \mathbf{R}^2$ and $t \in \mathbf{R}^+$. We note that the above formulation can be applied to dimensions higher than $\mathbf{R}^2$ without loss of generality. The situation is illustrated in Fig. 6.

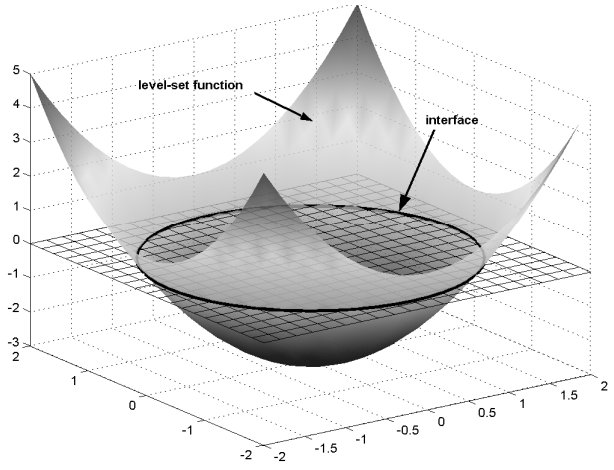

Figure 5: Representation of an interface by an implicit function.

Now, we suppose that the interface, $\Gamma(t)$ is moving with velocity $\boldsymbol{v}(\boldsymbol{x}, t)$. Since the interface is defined by

$$\phi\left(\boldsymbol{x}(t), t\right) = 0, \tag{2.5}$$

we can take the total derivative and obtain:

$$\frac{\mathrm{d}\phi\left(\boldsymbol{x}(t), t\right)}{\mathrm{d}t} = 0 \ , \tag{2.6}$$

$$\frac{\partial\phi}{\partial x}\frac{\mathrm{d}x}{\mathrm{d}t} + \frac{\partial\phi}{\partial y}\frac{\mathrm{d}y}{\mathrm{d}t} + \frac{\partial\phi}{\partial t} = 0 \ , \tag{2.7}$$

$$\frac{\partial\phi}{\partial t} + \boldsymbol{v}\cdot\nabla\phi = 0 \ , \tag{2.8}$$

$$\frac{\partial\phi}{\partial t} + v_n|\nabla\phi| = 0 \ , \tag{2.9}$$

where in (2.8) and (2.9), we have made use of the following relations,

$$\nabla\phi = |\nabla\phi|\boldsymbol{n} \ , \ \text{and} \tag{2.10}$$

$$v_n = \boldsymbol{v}\cdot\boldsymbol{n} \ , \tag{2.11}$$

respectively. We note that $v_n(\boldsymbol{x}, t)$ represents the normal velocity at a certain point $\boldsymbol{x}$ on the moving interface $\Gamma(t)$. Equation (2.9), which represents an advection equation for the moving interface, is also known as the *level-set equation*. It was first introduced by Osher and Sethian [50] for numerical interface evolution.

An important property of the interface, especially in two-fluid flow problems, is the mean curvature of the interface, defined as the divergence of the normal $\boldsymbol{n}$ as

$$\kappa\left(\boldsymbol{x}(t),t\right) = \nabla \cdot \boldsymbol{n} \ . \tag{2.12}$$

Substituting $\boldsymbol{n}$ from (2.10) into (2.12), we obtain

$$\kappa\left(\boldsymbol{x}(t),t\right) = \nabla \cdot \left(\frac{\nabla\phi}{|\nabla\phi|}\right) \ , \tag{2.13}$$

which represents the expression for the mean curvature defined in terms of the level-set function ϕ.

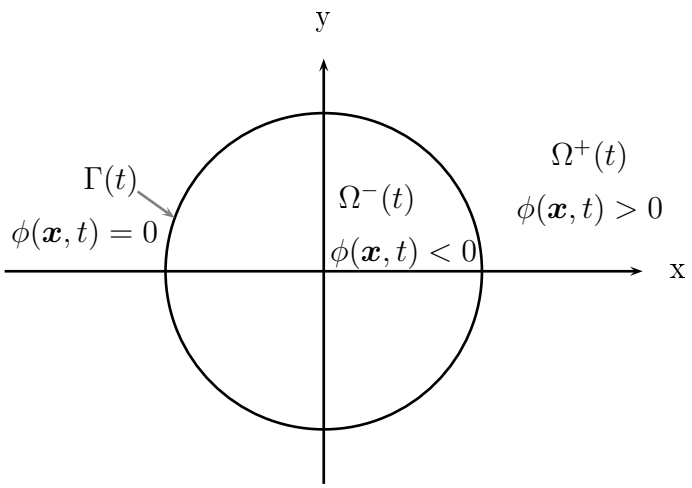

Figure 6: Separation of the $\mathbf{R}^2$ plane into domains $\Omega^-(t)$ and $\Omega^+(t)$ by the zero contour of the level-set function defined in (2.2) .

We now discuss a popular class of functions used for implicit surface representations known as the *signed-distance functions*. A distance function is defined as:

$$\phi_d\left(\boldsymbol{x}(t),t\right) = \min\|\boldsymbol{x}-\boldsymbol{x}_\Gamma\| \ , \quad \forall \boldsymbol{x}_\Gamma \in \Gamma \ \text{ and } \ \forall \boldsymbol{x} \in \mathbf{R}^n \ . \tag{2.14}$$

The distance function, ϕ_d is a legitimate level-set function since $\phi_d = 0 \ , \forall \boldsymbol{x} \in \Gamma$. Geometrically, for each point $\boldsymbol{x} \in \mathbf{R}^n$, the value of ϕ_d is simply the shortest distance of the point from the interface, Γ. A desirable property of the distance function is that

$$|\nabla\phi_d| = 1 \tag{2.15}$$

which immediately leads to the following simplications in the level-set equation (2.9) and the expression for the curvature (2.13),

$$\frac{\partial \phi}{\partial t} + v_n = 0 \ , \tag{2.16}$$

$$\kappa\left(\boldsymbol{x}(t), t\right) = \Delta\phi \ , \tag{2.17}$$

where $\Delta = \nabla \cdot \nabla$ is the *Laplacian* operator. A main disadvantage of using distance functions as the level-set function is that they possess a kink at the interface where $\phi_d = 0$ is a local minimum. This causes problems in approximating derivatives on or near the interface in a discrete setting. To overcome this problem, the signed-distance function is proposed and is defined as

$$\phi_{sd}\left(\boldsymbol{x}(t), t\right) \begin{cases} = -\phi_d & \forall \boldsymbol{x} \in \Omega^-(t) \\ = \phi_d & \forall \boldsymbol{x} \in \Omega^+(t) \\ = \phi_d = 0 & \forall \boldsymbol{x} \in \Gamma(t) \ . \end{cases} \tag{2.18}$$

A more compact definition is

$$\phi_{sd}\left(\boldsymbol{x}(t), t\right) = \pm \min \|\boldsymbol{x} - \boldsymbol{x}_\Gamma\| \ , \quad \forall \boldsymbol{x}_\Gamma \in \Gamma \ \text{ and } \ \forall \boldsymbol{x} \in \mathbf{R}^n \ , \tag{2.19}$$

where the correct sign to be taken is determined from (2.18). The signed-distance function also possesses the desirable property (2.15) and in addition, is monotone across the interface. This means that problems in differentiation at or near the interface disappear. The signed-distance representation of the interface in (2.3) is shown in Fig. 7.

2.3 Localization, Interpolation and Reinitialization

We have derived the basic level-set equation (2.9) in the preceding section while considering the simple example of a circular interface. In this section, we will discuss practical issues that arise in the discrete representation of the interface by the level-set method.

We first consider the issue of *localization*. We assume that our level-set function is defined in the $\mathbf{R}^2$ space, though our discussions apply equally well to higher dimensional spaces with straightforward generalization. In a standard discretization of the level-set function, the

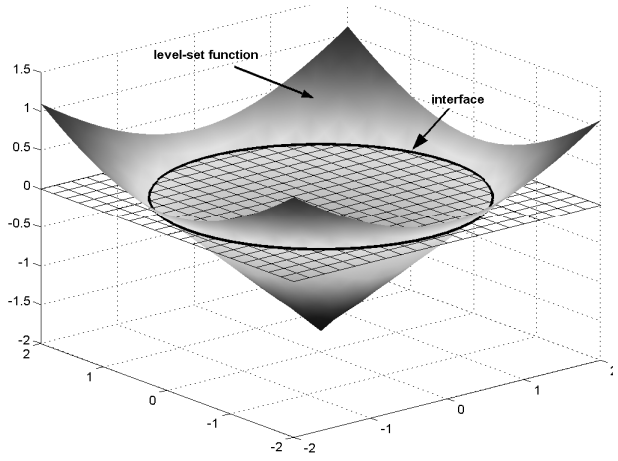

Figure 7: Representation of an interface by the signed-distance function.

values of the function are stored at the nodal points and the location of the interface needs to be interpolated from such nodal values. The standard way is to discretize the level-set function (2.19) in the entire computational domain D which is a subset of the $\mathbf{R}^2$ space, i.e. $D \subset \mathbf{R}^2$. However, this is unnecessary since all we need is to accurately locate the interface position and as such, points far away from the interface which do not contribute to the interpolation can be discarded. This leads to a *localization* strategy which means explicitly discretizing only at points very close to the interface, leaving the rest of D unresolved. Care must, however, be taken in the localization procedure since it has been reported that boundary stability problems do arise at the boundary within which localization is carried out (see e.g. Adalsteinsson and Sethian [1]). A recent localization method proposed by Peng *et al.* [51] effectively eliminates such boundary oscillations by incorporating a *cut-off* function in the level-set equation which causes the speed of evolution of the interface to decrease smoothly to zero at the boundary. We shall now outline some pertinent ideas from this work in the following paragraphs.

In [51], a standard Cartesian mesh with constant mesh sizes, Δx and Δy is employed. We define two constants, β and γ such that $\gamma > \beta > 0$ and which are comparable to the magnitude of Δx. Around the interface Γ, we define a tube with width γ by

$$T^0 = \{\boldsymbol{x} : |\phi^0(\boldsymbol{x})| < \gamma\} \ , \tag{2.20}$$

where ϕ^0 is the initial level-set function satisfying (2.9). We usually choose ϕ^0 to be a signed-distance function as this will simplify the level-set equation to take the form of

(2.16). We further define $c(\phi)$ to be a cut-off function such that:

$$c(\phi) = \begin{cases} 1 & \text{if } |\phi| \leq \beta \\ \frac{(|\phi|-\gamma)^2(2|\phi|+\gamma-3\beta)}{(\gamma-\beta)^3} & \text{if } \beta < |\phi| \leq \gamma \\ 0 & \text{if } |\phi| > \gamma \ . \end{cases} \tag{2.21}$$

Γ^0 is then updated by solving the following modified form of (2.9):

$$\frac{\partial \phi}{\partial t} + c(\phi) v_n |\nabla \phi| = 0 \ , \tag{2.22}$$

with initial data $\phi^0(\boldsymbol{x})$. The cut-off function is introduced to suppress numerical oscillations at the tube boundary. The original level-set equation (2.8) is only solved in the region $\{\boldsymbol{x} : |\phi^0(\boldsymbol{x})| < \gamma\}$ and the modified level-set equation (2.22) is solved in the region $\{\boldsymbol{x} : \beta < |\phi^0(\boldsymbol{x})| < \gamma\}$. Outside the tube Γ^0, the level-set function is not updated. The cut-off function $c(\phi)$, together with the relative positions of parameters, β and γ are illustrated in Fig. 8 for a simple one dimensional case.

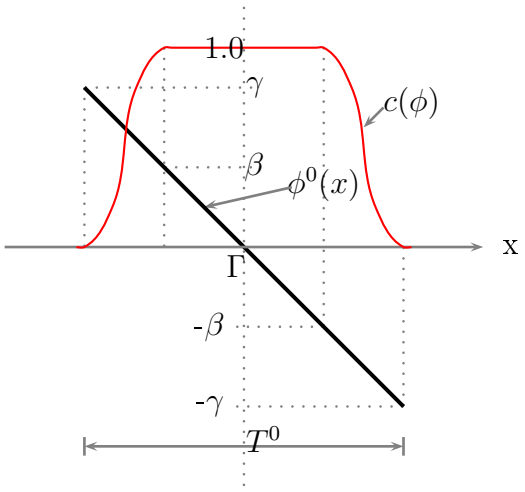

Figure 8: Illustration of cut-off function, $c(\phi)$ and relative positions of parameters, β and γ. $\phi^0(\boldsymbol{x})$ is the initial signed-distance function through the interface Γ.

We note that the implicit discretization of the level-set function does not tell us where the interface is located. To locate the interface, the $\phi(\boldsymbol{x}) = 0$ isocontour needs to be interpolated from the known discrete values of the level-set function $\phi_i = \phi(\boldsymbol{x}_i)$ at the nodal points where they are stored. In the XFEM literature, a standard linear FEM

approximation is typically used. In that case, the level-set function is interpolated by

$$\phi^h(\boldsymbol{x}) = \sum_{i \in I} N_i^{\mathrm{FEM}}(\boldsymbol{x})\,\phi_i \tag{2.23}$$

using standard FE shape functions N_i^{FEM} as interpolation functions. I is the set of all nodes in Ω. Of course, in a *localized* approach, I will then be the set of all nodes in a tube T^0 surrounding the interface. The representation of the discontinuity as the zero-level of $\phi^h(\boldsymbol{x})$ is only an approximation of the real position, which improves with mesh refinement.

An important point to note is that if bi-linear interpolation functions are used in (2.23), then in the cut elements, it is a good idea to rather subdivide the quadrilateral elements into two triangles and employ linear interpolation functions in each. This is done since three points uniquely define a plane. Therefore, the zero-level of $\phi^h(\boldsymbol{x})$, i.e. the representation of the interface, remains piecewise linear.

At the beginning of the simulation, the level-set function ϕ is initialized to be the signed-distance function ϕ_{sd} to the interface Γ^0. However, as the interface evolves with time, the level-set function may become very steep or flat in some regions, particularly in the vicinity of the interface, thus losing the desirable property, $|\nabla\phi| = 1.0$. This deterioration of the level-set function is inevitable and is a natural consequence of the advection process. but it makes an accurate determination of the interface difficult. We illustrate this difficulty with respect to Fig. 9 which shows the level-set function being advected in a single time step within a computational cell. Initially, the level-set function is initialized to be the signed-distance function, i.e. $\phi^0 = \phi_{sd}$. After one time step, the interface has shifted to position Γ^1 which is unknown to us since only the nodal values of the new level-set function ϕ^1 are stored. If we employ a linear interpolation (shown as a red line in Fig. 9) to approximate the position of the interface from the nodal level-set values, we will obtain $\tilde{\Gamma}^1$ which is not equal to the real interface position at Γ^1. We note that the closer the level-set function is to the signed-distance function, the better is the approximation. This provides the motivation for reinitializing the level-set function after each time step, in addition to obtaining simpler expressions for the level-set equation and the mean curvature. We also note that in the vicinity of the interface, where the level-set function is too steep, the interface propagation problem amounts to the transport of a nearly discontinuous function, which requires special discontinuity capturing (use of high-resolution schemes) to suppress numerical oscillations near the interface [37]. Those oscillations affect not only interface shape but also the quality of interface normal and curvature calculations.

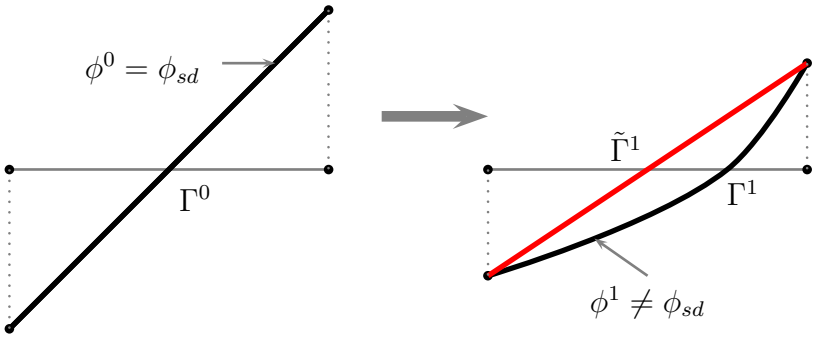

Figure 9: Movement of the level-set function within a computational cell in a single time step.

Reinitialization of the level-set function has been an active area of research in the level-set method (see e.g. [68, 78, 66, 51]). Reinitialization is simply the process of replacing ϕ by the signed-distance ϕ_{sd} which has the same zero contour as ϕ but is well-behaved (possessing the desired property,$|\nabla\phi| = 1.0$), and then taking this new function as the initial data to be used until the next round of reinitialization.

A straightforward way to reinitialize the level-set function is to locate the position of the interface by some interpolation technique and then construct the signed-distance function to this interpolated front (see, e.g. [6]). The accuracy of the approximated interface location depends on the accuracy of the interpolation method used. However, this procedure has the disadvantage that it may introduce unwanted oscillations in the curvature (which is needed to approximate the surface tension in two-fluid flows) [30]. This is highly undesirable in situations where such geometric quantities play a crucial role.

In Sussman *et al.* [68], the reinitialization is formulated as solving a partial differential equation together with initial condition given by

$$\frac{\partial\phi}{\partial t} + \mathrm{sgn}(\phi)(|\nabla\phi| - 1) = 0 \ , \ \forall(\boldsymbol{x}, t) \in \Omega \ \mathrm{X} \ (0, T_{steady}) \ , \tag{2.24}$$

$$\phi(\boldsymbol{x}, 0) = \phi^0 \ , \tag{2.25}$$

where ϕ^0 is the initial level-set function at the beginning of each time step. The above equation is to be solved to steady state where T_{steady} is the time taken to reach steady state. We note that at steady state, $\frac{\partial\phi}{\partial t} = 0$ and hence, $|\nabla\phi| = 1.0$. In principle, ϕ remains

unchanged at the interface (where $\text{sgn}(\phi) = 0$) and, therefore, the zero isocontour of ϕ and ϕ^0 are the same. Away from the interface, $|\nabla\phi|$ will converge to 1.0. This algorithm avoids explicitly locating the position of the interface by interpolation.

There exist a few problems with the above procedure. The sign function $\text{sgn}(\phi)$ has to be regularized in a discrete setting and this leads to numerical diffusion which will result in some inaccuracy in the location of the interface [71]. Also, as has been reported by Sussmann and Fatemi [66], in numerical approximations of (2.24), it has become evident that the zero isocontour will move, especially when the initial ϕ^0 is far from being a signed-distance function. They proposed a modification to the above reinitialization procedure where a constraint is added to the reinitialization such that the area (if ϕ is defined in $\mathbf{R}^2$ space) bounded by the zero isocontour could be approximately conserved locally within each cell. Though the zero isocontour might still move, the area bounded by the zero isocontour will be approximately preserved during the reinitialization. Other modifications to the original procedure include Peng *et al.* [51] who restricted the reinitialization procedure to within a tube (as discussed earlier) around the interface, thereby saving computational storage and time. They further noted that when ϕ_0 is very steep near the interface, the evolution to steady state might change the sign of ϕ_0, thus moving the interface across grid points. They proposed a new approximation to the $\text{sgn}(\phi)$ function different from that in [68] to ensure that the interface does not move across grid points.

3 The Extended Finite Element Method

The Extended Finite Element Method (XFEM) is a numerical method for modelling arbitrary discontinuities in finite elements by extending the piecewise polynomial approximation space of the standard FEM to include discontinuous function spaces in local regions of the computational domain which exhibit discontinuities. This is achieved via a partition-of-unity concept. In this section, the XFEM is described in detail along with its applications to various problems in physical science and engineering.

3.1 An Overview of the XFEM

For physical problems with smooth solutions, the piecewise continuous polynomial function space of the standard finite element method is usually sufficient to yield good results.

However, when solutions possess kinks, jumps, singularities, etc., standard finite element approximations require considerable mesh refinements if the element edges are not aligned with the discontinuities. The situation is even worse if the discontinuity evolves with time. Then, a constant remeshing is required throughout the simulation.

For the past decade, the need to model fracture processes (cracks in concrete, fatigue crack in adhesive bonded joints, etc.) has provided the impetus for the development of a new finite element technique based on the *Partition-of-Unity* (PUM) concept [8] to model cracks and crack growth which do not require any remeshing. The idea is to take into account *a priori* known discontinuous solution properties and incorporating them as non-classical shape functions into the standard FEM approximation space via a partition-of-unity concept. Finite element shape functions are used to build a partition of unity and to localize the involved enrichment functions. As such, the XFEM is often called a *local* PUM method.

The idea was first conceived by Belytschko and Black [12] who achieved minimal remeshing for the finite element method by adding discontinuous asymptotic crack tip displacement enrichment functions to the FEM approximation space in order to account for the presence of the cracks. However, curved cracks were treated by a tedious mapping of the straight crack enriched field and hence, their method is not readily applicable to long cracks or cracks in three dimensions. In Moës *et al.* [48], not only were the nodes enriched with the asymptotic crack tip displacement solutions near the crack tip, but also with a *step* function along the crack path which takes into account the jump of the displacement across the crack. The finite element mesh can then be defined independently of the crack geometry and no remeshing was required.

A significant advance of the XFEM was given by its coupling with the level-set method (see e.g. Stolarska *et al.* [59]). An advantage of this coupling is that the process of determining the nodes to be enriched is facilitated through the level set representation. The level-set method provides an excellent complement to the XFEM as both require only a fixed mesh to be used throughout the simulation.

Ever since the introduction of the XFEM in the pioneering works of Belytschko *et al.* [12] and Moës *et al.* [48], it has rapidly evolved into an extremely active and fruitful field of research with simulation results in XFEM presented for a multitude of physical problems including modelling of branched and intersecting cracks [25], holes and inclusions [63], dislocations [74], solidification problems [22, 26, 41], particulate flows (particle-laden flows) [76,

75], two-phase flows [19, 18], boundary layer problems [56], etc. See Table 1 (Section 3.5) for a list of XFEM applications.

One of the problems of the standard XFEM approximation is the existence of blending elements when certain enrichment functions were used (see e.g. [23, 31]). The origins of this problem along with its proposed solutions will be explained in more detail in Section 3.3.

Central to the development of the XFEM is the concept of an approximation space. In the following section, we shall explain the basic ideas of an enriched approximation space and how it naturally leads to the development of the XFEM.

3.2 The Formulation of the XFEM

In this section, we demonstrate that the XFEM arises naturally due to attempts in incorporating known solution properties into the standard FE approximation space, starting from the well-known Global-Local method [49]. Our arguments in this section are heuristic and intuitive rather than formal.

We first explain the difference between a weak discontinuity and a strong discontinuity with respect to the one-dimensional $\mathbf{R}$ line. A function $f : \Omega(a,b) \mapsto \mathbf{R}$ (for some real numbers a and b where $a < b$) is said to be of class $C^k(\Omega)$ if its derivatives of order j, where $0 \leq j \leq k$ exist and are continuous functions [54]. We shall be concerned with C^{-1}, C^0 and C^1 functions in particular. Examples of these are illustrated in Fig. 10. As can be seen, the C^0 function is piecewise continuously differentiable, i.e., its first derivative is continuous everywhere except at the point c where the derivative does not exist. This is called a point of *weak* discontinuity (also called a kink). The C^1 function is continuously differentiable everywhere in the entire domain $\Omega(a,b)$; i.e., its first derivative exists and is continuous everywhere in the domain $\Omega(a,b)$. The C^{-1} function is piecewise continuous except at the point, c where it is not continuous. It is said to exhibit a *strong* discontinuity (also called a jump) at the point c. We note further that the derivative of a C^0 function is a C^{-1} function and in general, the derivative of a C^n function is a C^{n-1} function.

Both weak and strong discontinuities inside elements can be incorporated into the FEM approximation space. To see how this can be done, we first consider the standard FEM

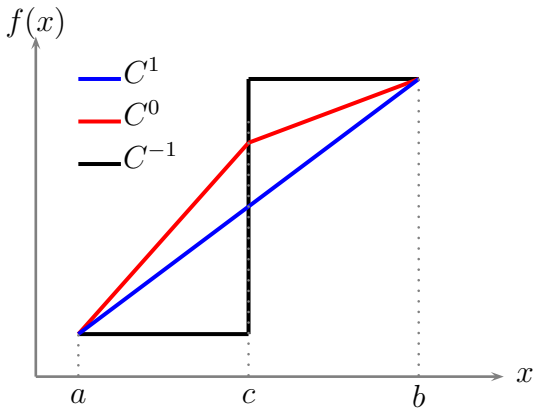

Figure 10: Illustration of C^{-1}, C^0 and C^1 functions.

approximation which takes the form

$$u^h(\boldsymbol{x}) = \sum_{i \in I} N_i^{\mathrm{FEM}}(\boldsymbol{x})\, u_i \ , \tag{3.1}$$

where the individual variables are defined as

$u^h(\boldsymbol{x})$	:	approximation function,
$N_i^{\mathrm{FEM}}(\boldsymbol{x})$	:	FE interpolation function at node i,
u_i	:	nodal unknown of the approximated function,
I	:	set of all nodes in the computational domain.

In a linear FEM approximation, $N_i^{\mathrm{FEM}}(\boldsymbol{x})$ are piecewise linear polynomials. The approximated function $u^h(\boldsymbol{x})$ will then also be piecewise linear. Within each element domain, $u^h(\boldsymbol{x})$ is C^1 but kinks (weak discontinuities) exist at interelement boundaries so that on the entire domain, $u^h(\boldsymbol{x})$ is C^0. It is then obvious that to model kinks in physical problems, the usual approach will be to align the element edges with the kinks since the approximated function already possesses a weak discontinuity at such interelement boundaries in the first place. However, if the element edges are not aligned with the kinks, the linear polynomial approximation space (with C^1 continuity) within each element will not be able to reproduce the C^0 discontinuity.

If we do not wish to take the hassle to align the element edges with the kinks, the only

logical solution seems to be to expand the original linear polynomial approximation space such that it is able to reproduce the weak discontinuity within the element. This provides the motivation for enriched finite element methods. The simplest way to enrich the FEM approximation space is to simply add an *enrichment* function to the standard FEM approximation. It is conceivable that the enrichment function should be chosen such that it possesses the same peculiar characteristics as the discontinuity to be modelled. For example, to model a kink, one would choose a function which possesses a kink as the enrichment function. One of the earliest enriched methods is called the *Global-Local* method [49] which takes the form

$$u^h(\boldsymbol{x}) = \sum_{i \in I} N_i(\boldsymbol{x})\, u_i + a g(\boldsymbol{x}) \ , \tag{3.2}$$

where $g(\boldsymbol{x})$ is the global enrichment function which is defined throughout the computational domain and a is an unknown coefficient. The function $g(\boldsymbol{x})$ should possess the desired non-polynomial characteristics (kinks, jumps, etc.) that are to be modelled. If there exist multiple discontinuities in the physical problem, we can simply add the respective enrichment functions to the standard FEM approximation:

$$u^h(\boldsymbol{x}) = \sum_{i \in I} N_i(\boldsymbol{x})\, u_i + \sum_{j=1}^{m} a_j g_j(\boldsymbol{x}) \ , \tag{3.3}$$

where m is the total number of enrichment functions. This method, though conceptually simple, has three important deficiencies. First, since $g(\boldsymbol{x})$ is defined globally, this would mean additional storage even in regions of the domain where the enrichment is not needed and where the standard polynomial approximation space suffices. This not only leads to computational inefficiency but also effectively destroys the sparseness property of the standard FEM stiffness matrix. Second, the use of a single degree-of-freedom (parameter), a, in realizing the shape of the enrichment function leads to a serious restriction in the different shapes of the discontinuity that can be represented, especially for problems in two dimensions or higher. Finally, using approximation (3.3), one can no longer satisfy the patch test for any $a_j \neq 0$. The first problem can be resolved simply by setting the values of $g(\boldsymbol{x})$ to be zero in those parts of the domain where the enrichment is not needed, thereby localizing the enrichment and retaining the sparseness property. The second problem provides the motivation for the development of the highly successful Partition-of-Unity Method (PUM) [45, 9], which, in turn, leads to the development of the XFEM.

The PUM approximation takes the form

$$u^h(\boldsymbol{x}) = \sum_{i \in I} N_i(\boldsymbol{x}) \left[u_i + a_i g(\boldsymbol{x}) \right] , \tag{3.4}$$

where it can be seen that the enrichment function $g(\boldsymbol{x})$ is pre-multiplied by the term, $\sum_{i \in I} N_i(\boldsymbol{x}) a_i$. This is done so that $g(\boldsymbol{x})$ can now be more flexibly adjusted within each element to fit the solution at hand. Also, $g(\boldsymbol{x})$ can be represented exactly since the shape functions multiplying $g(\boldsymbol{x})$ form a partition-of-unity in the entire domain, i.e.

$$\sum_{i \in I} N_i(\boldsymbol{x}) = 1 . \tag{3.5}$$

This is in contrast to the Global-Local method where a single parameter a is used for all elements for one enrichment. The PUM has been put on a rigorous mathematical foundation by Babuška and Melenk [8]. One drawback of the PUM is that the enrichment function, similar to the Global-Local method, is defined globally. As again, this can be circumvented by setting the values of $g(\boldsymbol{x})$ to be zero in those parts of the domain where the enrichment is not needed. It is interesting to note that, this procedure, though simple, has been ignored by the majority of the XFEM community. As we shall see, knowledge of this simple fact will effectively eliminate the parasitic terms in the blending elements, a problem which has plagued the XFEM community until only recently [31].

The PUM can be seen as the precursor to the XFEM. In fact, the XFEM has often been seen as a *local* PUM approach where *local* here means the enrichment function is confined to a local region of the domain by using the partition-of-unity functions as a window to restrict the global enrichment function to the subdomain where the enrichment is needed. The standard XFEM approximation is given as:

$$u^h(\boldsymbol{x}) = \sum_{i \in I} N_i(\boldsymbol{x}) u_i + \sum_{i \in I^*} N_i^*(\boldsymbol{x}) a_i g(\boldsymbol{x}) , \tag{3.6}$$

where the individual variables are defined according to

$$\begin{aligned} u^h(\boldsymbol{x}),\ N_i(\boldsymbol{x}),\ u_i,\ I \quad &: \quad \text{defined as in (3.1),} \\ N_i^*(\boldsymbol{x}) \quad &: \quad \text{partition-of-unity function at node } i, \\ a_i \quad &: \quad \text{unknown of the enrichment at node } i, \end{aligned}$$

$$
\begin{aligned}
I^* \quad &: \quad \text{nodal subset of the enrichment, } I^* \subset I, \\
g(\boldsymbol{x}) \quad &: \quad \text{global enrichment function.}
\end{aligned}
$$

We can see immediately, by comparing (3.6) and (3.4), that the main difference between the two is the use of a mere subset, $I^* \subset I$, in the enrichment term in the XFEM approximation (3.6). This means that only certain nodes in a subdomain, $I^* \subset I$, are enriched. We note that such a procedure has not been mathematically justified. Despite this, the XFEM has been successfully applied to a wide range of physical problems including those with discontinuities in the function [14, 48, 25, 27] and those with discontinuities in the derivatives [22, 26, 19, 41]. We shall discuss in more detail in the next section how such a procedure of using just a subset, $I^* \subset I$, in the enrichment term may lead to the well-known problem of suboptimal convergence rates due to parasitic terms introduced by the existence of the blending elements [23, 31].

An important question remains as to which nodes should be included in the subset, $I^* \subset I$ in the above approximation? We shall answer this question with reference to Fig. 11 where a cartesian grid in two dimensions is crossed by a curved discontinuity. In order to reproduce the discontinuity in the shaded elements (also called *reproducing* elements), we need the parition-of-unity functions, $N_i^*(\boldsymbol{x})$ to build a partition-of-unity over such elements. The only way to realize this is to include all the surrounding nodes of such elements in the nodal set, I^* shown as dark-colored dots in the figure.

A more general form of the XFEM approximation for multiple enrichments is given by:

$$
u^h(\boldsymbol{x}) \;=\; \sum_{i \in I} N_i(\boldsymbol{x})\, u_i + \sum_{j=1}^{m} \sum_{i \in I_j^*} N_i^*(\boldsymbol{x})\, a_i^j g^j(\boldsymbol{x}) \quad , \tag{3.7}
$$

where the individual variables are defined according to

$$
\begin{aligned}
u^h(\boldsymbol{x}),\ N_i(\boldsymbol{x}),\ u_i,\ I \quad &: \quad \text{defined as in (3.1)}, \\
N_i^*(\boldsymbol{x}),\ I^* \quad &: \quad \text{defined as in (3.6)}, \\
a_i^j \quad &: \quad \text{unknown of the enrichment } j \text{ at node } i, \\
I_j^* \quad &: \quad \text{nodal subset of enrichment } j,\ I_j^* \subset I, \\
g^j(\boldsymbol{x}) \quad &: \quad j^{th} \text{ global enrichment function.}
\end{aligned}
$$

If only one enrichment is used, (3.7) reverts to (3.6). We further note that for each

enrichment, the PU functions $N_i^*(\boldsymbol{x})$ build a partition-of-unity in the corresponding local part of the domain where the enrichment is desired to be reproduced, i.e.

$$\sum_{i \in I_j^*} N_i^*(\boldsymbol{x}) = 1 \quad \forall \boldsymbol{x} \in \Omega_j^*, \quad \forall j = 1, \cdots, m, \tag{3.8}$$

where the domain, Ω_j^* is the union of all the reproducing elements attached to enrichment j.

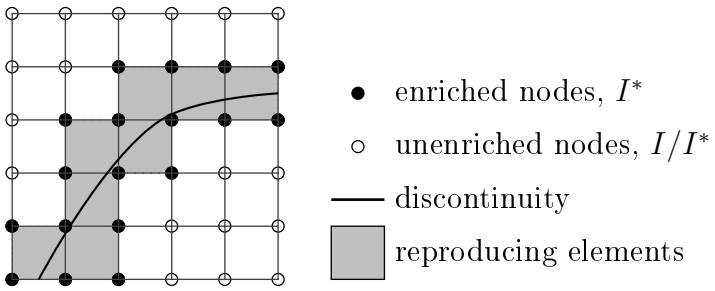

Figure 11: Discretized domain crossed by a curved discontinuity in two dimensions displaying the nodal set I^* and the reproducing elements.

3.3 Problems in Blending Elements

In the previous section, we have given the standard formulation of the XFEM and have suggested that the PUM may be seen as the logical foundation of the XFEM. We adopt the point of view that the XFEM is a special case of the PUM. As such, we need no longer worry about the mathematical justification of the XFEM as it conveniently inherits all the essential mathematical properties of the PUM which has already been rigorously justified in earlier works [8, 45, 9]. As we shall see later in the section, this point of view provides invaluable insight into the origins of the well-known problems in the blending elements and enables us to look for straighforward remedies without recourse to more complicated techniques such as the Assumed Strain XFEM [23] or the Discontinuous-Galerkin XFEM [34]. Our task now is to reconcile the standard XFEM formulation with the original PUM formulation and show how the former arises as a *legitimate* special case of the latter.

As mentioned in the previous section, the discrete equations are not sparse in the original PUM since the global enrichment function is defined globally. However, this problem

can be easily resolved simply by setting the values of $g(\boldsymbol{x})$ to be zero in those parts of the domain where the enrichment is not needed, thereby localizing the enrichment and retaining the sparseness property. However, this seemingly trivial procedure is not as simple as it seems. To illustrate this, we consider a simple one-dimensional problem in which the *abs-enrichment* is used to reproduce a weak discontinuity (i.e. kink) in an element (see Fig. 12). The line in blue shows the new localized enrichment function. It is seen that the original global enrichment function is set to zero everywhere except on the element where the kink exists. This element is also called the *reproducing element* since the kink is to be *reproduced* in this element. However, such a localized enrichment is inadmissible; the reason being that strong discontinuities in the localized enrichment function now exist at the element edges (nodes in this 1-D case) of the enriched element. However, an FE solution with Lagrange polynomials requires that C^0-continuity is observed at the interelement boundaries (nodes). This leads to a direct contradiction which renders the solution impossible. An alternative localized enrichment function is shown in Fig. 13, where it can be observed that only weak discontinuities (C^0-continuity) in the enrichment function exist at both nodes of the enriched element [47]. This does not violate the requirement of C^0-continuity at the nodes. Hence, it is an admissible localized enrichment function.

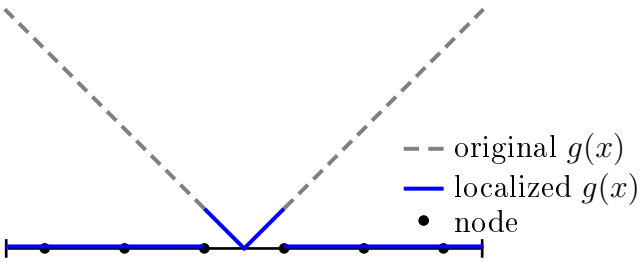

Figure 12: An inadmissible localization of the global enrichment function, $g(x)$ in the PUM.

In view of the above modification to the global enrichment function, we now rewrite our original PUM apoproximation (3.4) as

$$u^h(\boldsymbol{x}) = \sum_{i\in I} N_i(\boldsymbol{x})\, u_i + \sum_{i\in I^*} N_i^*(\boldsymbol{x})\, a_i g(\boldsymbol{x}) \quad , \tag{3.9}$$

where the partition-of-unity functions, $N_i^*(\boldsymbol{x})$ in the second term on the RHS of (3.9) builds a partition-of-unity only over those elements whose nodes are all included in the subset,

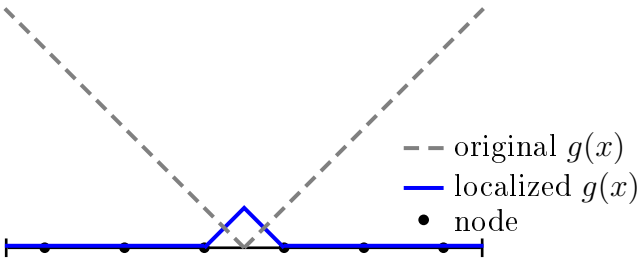

Figure 13: An admissible localization of the global enrichment function, $g(x)$ in the PUM.

$I^* \subset I$ and $g(\boldsymbol{x})$ is the new localized enrichment function. The transition from (3.4) to (3.9) is justified since the enrichment function is only non-zero over the enriched elements whose surrounding nodes are included in the subset, I^* in (3.9). Though the above Local PUM approximation is very similiar to the standard XFEM approximation (3.6), the subtle difference lies in the way in which the global enrichment function is constructed. In the XFEM, we employ the partition-of-unity functions as a window to localize the enrichment function without first imposing any condition on the form of the enrichment function. This is in contrast to the Local PUM where we first choose an *admissible* localized enrichment function and then apply an appropriate partition-of-unity to those parts of the domain where the localized enrichment function is non-zero. As we shall see, this seemingly trivial difference can lead to problematic *side effects* in the XFEM approximation, manifested as parasitic terms in the blending elements.

An advantage of the Local PUM over the standard XFEM is that for the Local PUM, the computed unknowns are directly the sought function values, i.e.

$$u^h(\boldsymbol{x}_i) = u_i \quad . \tag{3.10}$$

This is a consequence of the FEM shape functions possessing the Kronecker-δ property,

$$N_i(\boldsymbol{x}_j) = \delta_{ij} = \begin{cases} 0 & : i \neq j \\ 1 & : i = j \end{cases} \quad , \tag{3.11}$$

and that the localized global enrichment function is zero at all nodes. This facilitates the imposition of Dirichlet boundary conditions in the Local PUM. In the standard XFEM, however, shifting of the global enrichment function needs to be performed in order to

preserve the property in (3.10).

The only disadvantage of the Local PUM is that it is not always easy to contruct an admissible localized global enrichment function, especially in dimensions higher than two. For the standard XFEM, the global enrichment function for a weak discontinuity can be conveniently constructed with the aid of the level-set function as:

$$g(\boldsymbol{x}) = \text{abs}(\phi(\boldsymbol{x})) = |\phi(\boldsymbol{x})| \ , \tag{3.12}$$

where $|\cdot|$ is the absolute function. The global enrichment function for a strong discontinuity can also be easily constructed with the aid of the level-set function as:

$$g(\boldsymbol{x}) = \text{H}(\phi(\boldsymbol{x})) = \begin{cases} 0 & : \phi(\boldsymbol{x}) \leq 0 \\ 1 & : \phi(\boldsymbol{x}) > 0 \end{cases} \ , \tag{3.13}$$

where $\text{H}(\cdot)$ is the Heaviside function. Similar definitions for the Local PUM are not as straightforward, especially in dimensions higher than two. One needs to ensure that the enrichment function not only possesses the desired discontinuity within the reproducing elements but also that it is zero outside the reproducing elements.

In the XFEM, the procedure of restricting the enriched nodes to just a subset, $I^* \subset I$ is motivated by the desire to keep the discrete equations sparse as opposed to the original PUM where the system is not sparse since the global enrichment function is indeed defined globally. One obvious consequence of this modification to the PUM is that the partition-of-unity functions, $N_i^*(\boldsymbol{x})$ no longer build a partition-of-unity in the entire domain. In fact, they build a partition-of-unity only over the *enriched* elements whose nodes are all in the subset, I^*. Elements which have only some of their nodes within the subset, I^* are called *blending* elements. Elements which have none of their nodes in the subset, I^* are the standard finite elements. We note that since the partition-of-unity functions build a partition-of-unity over the enriched elements, these elements are able to reproduce the discontinuities embedded in the global enrichment function. Hence, they are also called *reproducing* elements. The blending elements act as *transition* elements between the reproducing elements and the standard unenriched finite elements. The situation is illustrated in Fig. 14.

Two inevitable consequences arise when the PU functions do not build a partition-of-unity over the blending elements. First, the enrichment function can no longer be reproduced over the blending elements. This is trivial since the discontinuity has never been intended

to be reproduced over the blending elements in the first place. Second, and more importantly, unwanted parasitic terms are introduced in the enrichment term which cannot be compensated by the standard FE part of the XFEM approximation. For example, in an XFEM approximation utilizing linear interpolation and PU functions, quadratic terms are produced by the enrichment term in the blending elements when the abs-enrichment is used and these cannot be cancelled by the standard FE part which contains only linear terms (see e.g. [31]).

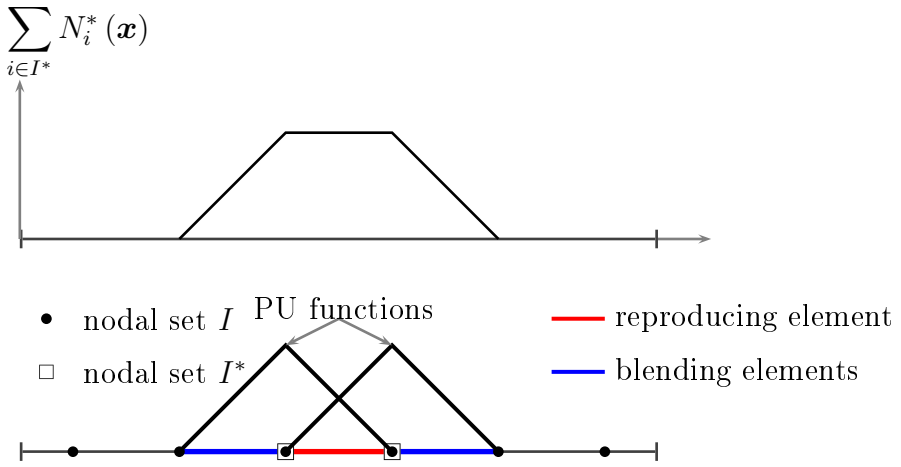

Figure 14: Illustration of reproducing and blending elements. PU functions build a partition-of-unity only over the reproducing element.

Problems with the blending elements in XFEM were first reported by Sukumar *et al.* [63] who observed suboptimal convergence rates when the abs-enrichment is used for discontinuous derivatives. Subsequent works aimed at addressing this problem include Chessa *et al.* [23] who developed the Enhanced Strain-XFEM (ES-XFEM) method , Fries [31] who proposed the corrected-XFEM approximation and Gracie *et al.* [34] who proposed the Discontinuous Galerkin-XFEM (DG-XFEM) method. We will describe each of these methods in more detail below.

The ES-XFEM proposed by Chessa *et al.* [23] is a variant of Assumed Strain method [55], which is based on the *Hu–Washizu* variational principle. The enhanced strain elements are used only in the blending domain. The enhanced strain field is designed so that it can eliminate the undesirable terms that arise from the enrichment function in the blending subdomain. It can be used for arbitrary enrichment functions. The primary drawback of

the ES-XFEM is the difficulty in constructing the basis functions for the ES approximation. The functions must be linearly independent and span the space of the parasitic terms and furthermore must be constructed for each choice of enrichment. Thus, it lacks generality and ease of implementation.

In the DG-XFEM method, the domain is decomposed into patches where enrichments are to be added. Each patch is discretized independently. Enrichments are applied over entire patches but not over the entire domain. As a result, the enrichment is local but there is no need for blending elements. Continuity between the patches is enforced in a weak sense using the Internal Penalty (IP) method of Wheeler [77]. Both a patch-based version of the DG formulation and an element-based version are developed. The patch-based version decomposes the domain into enriched and unenriched subdomains. The element-based form considers each element as a patch. The patch-based DG is shown to have similar accuracy to the element-based DG for a given discretization but requires significantly fewer degrees of freedom. Although this method works for arbitrary enrichments, it is not conceptually simple and requires plenty of computational effort especially in subdividing the domain into patches and enforcing the continuity between the patches.

The Corrected-XFEM of Fries [31] possesses both generality and ease of implementation. It is motivated by the realization that the global enrichment function can be localized and thereby eliminating the parasitic terms produced by the blending elements from the outset. In this method, all nodes in the blending elements are enriched and a ramp function is used to window the global enrichment function so that it decreases to zero in a continuous fashion over the blending elements. The method works for arbitrary enrichments and all element types. However, due to multiplication of the global enrichment function with the ramp function, more integration points are needed. Also, since more nodes are enriched, this leads to slightly more degrees of freedom and hence, more computational effort compared to the standard XFEM. Despite these shortcomings, the method is conceptually simple and can be easily implemented. We note that this method is very similar in its approach to the Local PUM proposed earlier; the only difference being that in the Local PUM, the global enrichment function is localized without utilizing a ramp function, thereby doing away with the need for more integration points and additional degrees of freedom.

We note that blending elements do not exist in the original PUM since the entire domain is enriched. That is, the PU functions build a partition-of-unity over the entire domain. In the Local PUM, the transition elements do not contribute any unwanted parasitic terms since the non-zero PU functions over the blending elements are multiplied by the zero

global enrichment function leading to an overall zero contribution from the enrichment term in the approximation. Therefore, any parasitic terms are eliminated from the outset. Fig. 15 compares the enrichment functions for both the Corrected-XFEM and the Local PUM for a one-dimensional case.

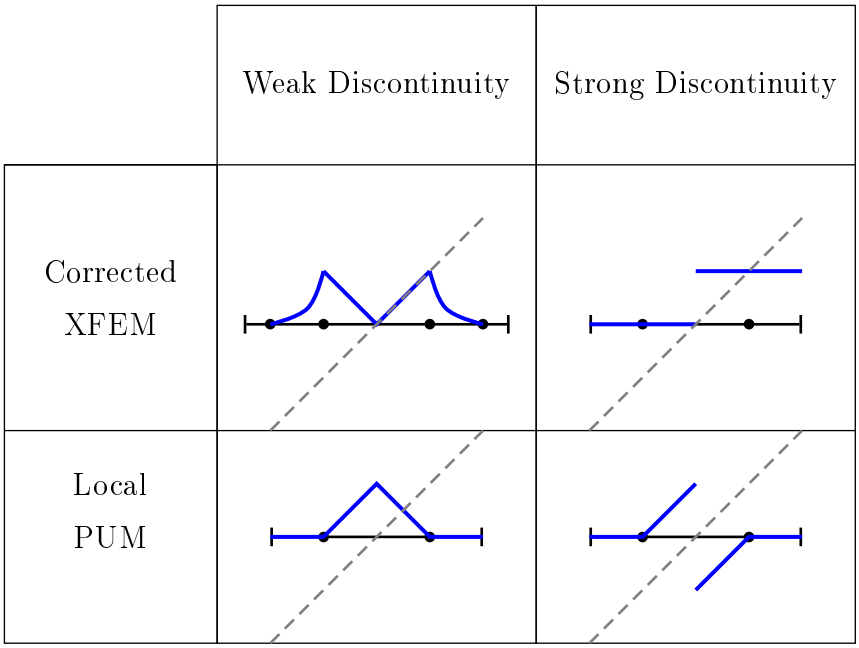

Figure 15: Comparison of enrichment functions for weak and strong discontinuities for both the Corrected-XFEM and the Local PUM. Dashed line shows the level-set function.

3.4 Derivation of the Weak Form

Central to an FE approximation is the development of the weak form of the partial differential equation (PDE) being modelled. In the following paragraphs, we will demonstrate the general methodology by which the weak form of a PDE with *discontinuous coefficients* can be derived from its corresponding strong form. For a standard exposition on the development of the weak form for smooth problems, the reader is referred to Hughes [40].

The model PDE chosen is the Laplace equation. We note that the notations used here follow closely those of Belytschko *et al.* [14]. We consider the Laplace equation with a

discontinuous coefficient, $\alpha(\boldsymbol{x})$ over a domain, Ω with boundary, Γ. The strong form is given by

$$\nabla \cdot (\alpha(\boldsymbol{x}) \nabla u(\boldsymbol{x})) = 0 \quad \text{on } \Omega \ , \tag{3.14}$$

with boundary conditions

$$[\alpha(\boldsymbol{x}) u(\boldsymbol{x})_{,N}] \equiv \alpha^+ \nabla u^+ \cdot \boldsymbol{n}^+ \ + \ \alpha^- \nabla u^- \cdot \boldsymbol{n}^- \ = \ 0 \quad \text{on } \Gamma_D \ , \tag{3.15}$$

$$u(\boldsymbol{x})_{,N} = \nabla u(\boldsymbol{x}) \cdot \boldsymbol{n} \ = \ 0 \quad \text{on } \Gamma_F^- \text{ and } \Gamma_F^+ \ , \tag{3.16}$$

$$\alpha(\boldsymbol{x}) u(\boldsymbol{x})_{,N} = \alpha(\boldsymbol{x}) \nabla u(\boldsymbol{x}) \cdot \boldsymbol{n} \ = \ h \quad \text{on } \Gamma_h \ , \tag{3.17}$$

$$u(\boldsymbol{x}) \ = \ g(\boldsymbol{x}) \quad \text{on } \Gamma_u \ , \tag{3.18}$$

where $\boldsymbol{n}$ is the unit normal vector to the surface, the superscripts '+' and '−' designate two sides of the interface and $\alpha(\boldsymbol{x})$ is a C^{-1} function along Γ_D and smooth otherwise. The solution possesses a strong discontinuity on Γ_F and a weak discontinuity on Γ_D. The situation is illustrated in Fig. 16.

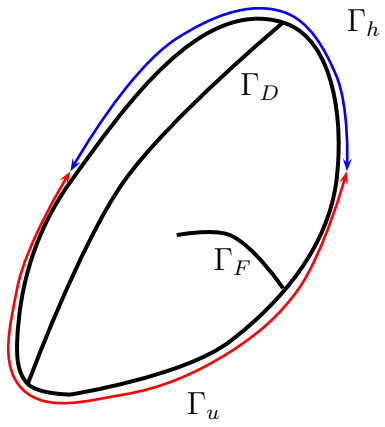

Figure 16: Domain, Ω containing a weak discontiuity on Γ_D and a strong discontinuity on Γ_F with natural boundary condition on Γ_h and essential boundary condition on Γ_u.

We now seek to derive the weak form from the above strong form. We first define the spaces where the trial and test functions reside, respectively

$$\mathcal{U} \ = \ \{u(\boldsymbol{x}) \mid u(\boldsymbol{x}) \in \mathcal{H}_1, \ u(\boldsymbol{x}) = g(\boldsymbol{x}) \text{ on } \Gamma_u, \ u(\boldsymbol{x}) \text{ discontinuous on } \Gamma_F\} \ , \tag{3.19}$$

$$\mathcal{U}_0 \ = \ \{\delta u(\boldsymbol{x}) \mid \delta u(\boldsymbol{x}) \in \mathcal{H}_1, \ \delta u(\boldsymbol{x}) = 0 \text{ on } \Gamma_u, \ \delta u(\boldsymbol{x}) \text{ discontinuous on } \Gamma_F\} \ , \tag{3.20}$$

where $\mathcal{H}_1$ denotes the *Sobolev space* defined as

$$\mathcal{H}_1(\Omega) = \{f \in L^2(\Omega);\ D^1 f \in L^2(\Omega)\}\ , \tag{3.21}$$

where D^1 denotes the partial differential operator and L^2 is the familiar space of square-integrable functions. We now multiply (3.14) by the test function, $\delta u(\boldsymbol{x})$ and integrate over the domain, Ω

$$\int_\Omega \delta u(\nabla \cdot (\alpha \nabla u))\,\mathrm{d}\Omega = 0\ . \tag{3.22}$$

But from the *product rule*

$$\nabla \cdot (\delta u \alpha \nabla u) = \delta u(\nabla \cdot \alpha \nabla u) + \alpha \nabla u \nabla(\delta u)\ , \tag{3.23}$$

which implies that (3.22) can be written as

$$\int_\Omega \delta u(\nabla \cdot (\alpha \nabla u))\,\mathrm{d}\Omega = \int_\Omega [\nabla \cdot (\delta u \alpha \nabla u) - \alpha \nabla u \nabla(\delta u)]\,\mathrm{d}\Omega = 0\ . \tag{3.24}$$

From the Divergence Theorem, we have

$$\int_\Omega \nabla \cdot (\delta u \alpha \nabla u)\,\mathrm{d}\Omega = \oint_\Gamma \boldsymbol{n} \cdot (\delta u \alpha \nabla u)\,\mathrm{d}\Gamma\ , \tag{3.25}$$

whereupon substitution into (3.24) yields

$$\int_\Omega \alpha \nabla u \nabla(\delta u)\,\mathrm{d}\Omega - \oint_\Gamma \boldsymbol{n} \cdot (\delta u \alpha \nabla u)\,\mathrm{d}\Gamma = 0\ . \tag{3.26}$$

Further, taking into account (3.17) and (3.20), (3.26) can now be written as

$$\int_\Omega \alpha \nabla u \nabla(\delta u)\,\mathrm{d}\Omega - \oint_{\Gamma_h} \delta u h\,\mathrm{d}\Gamma = 0\ . \tag{3.27}$$

The above equation represents the weak form of (3.14). A formal statement of the weak form is: Find $u \in \mathcal{U}$ such that (3.27) holds $\forall \delta u \in \mathcal{U}_0$. We now derive the strong form from the above weak form and prove that all the boundary conditions can be obtained as

by-products of the derivation. The first term of (3.27) can be written as

$$\int_\Omega \alpha \nabla u \nabla(\delta u)\,\mathrm{d}\Omega = \int_\Omega \nabla\cdot(\delta u \alpha \nabla u)\,\mathrm{d}\Omega - \int_\Omega \delta u(\nabla\cdot(\alpha\nabla u))\,\mathrm{d}\Omega \ . \tag{3.28}$$

The first term on the RHS of (3.28) can be written, using the Divergence Theorem, as

$$\begin{aligned}\int_\Omega \nabla\cdot(\delta u\alpha\nabla u)\,\mathrm{d}\Omega &= \oint_\Gamma \boldsymbol{n}\cdot(\delta u\alpha\nabla u)\,\mathrm{d}\Gamma \ , \\ &= \oint_{\Gamma_h} \boldsymbol{n}\cdot(\alpha\nabla u)\delta u\,\mathrm{d}\Gamma + \oint_{\Gamma_F\bigcup\Gamma_D} \boldsymbol{n}^+\cdot(\delta u\alpha\nabla u)^+\,\mathrm{d}\Gamma \\ &\quad + \oint_{\Gamma_F\bigcup\Gamma_D} \boldsymbol{n}^-\cdot(\delta u\alpha\nabla u)^-\,\mathrm{d}\Gamma \ .\end{aligned} \tag{3.29}$$

Since $\delta u^+ = \delta u^-$ on Γ_D as required by (3.20), we obtain

$$\begin{aligned}\int_\Omega \nabla\cdot(\delta u\alpha\nabla u)\,\mathrm{d}\Omega &= \oint_{\Gamma_h} \boldsymbol{n}\cdot(\alpha\nabla u)\delta u\,\mathrm{d}\Gamma \\ &\quad + \oint_{\Gamma_D} \delta u\Big(\boldsymbol{n}^+\cdot(\alpha\nabla u)^+ + \boldsymbol{n}^-\cdot(\alpha\nabla u)^-\Big)\,\mathrm{d}\Gamma \\ &\quad + \oint_{\Gamma_F} \Big(\boldsymbol{n}^-\cdot(\delta u\alpha\nabla u)^- + \boldsymbol{n}^+\cdot(\delta u\alpha\nabla u)^+\Big)\,\mathrm{d}\Gamma \ .\end{aligned} \tag{3.30}$$

Substituting (3.30) into (3.28) which is then substituted into the weak form (3.27), we obtain

$$\begin{aligned}-\int_\Omega \delta u(\nabla\cdot(\alpha\nabla u))\,\mathrm{d}\Omega + \oint_{\Gamma_h} \delta u(\boldsymbol{n}\cdot\alpha\nabla u - h)\,\mathrm{d}\Gamma + \oint_{\Gamma_D} \delta u[\alpha u_{,N}]\,\mathrm{d}\Gamma \\ + \oint_{\Gamma_F} \Big(\boldsymbol{n}^-\cdot(\delta u\alpha\nabla u)^- + \boldsymbol{n}^+\cdot(\delta u\alpha\nabla u)^+\Big)\,\mathrm{d}\Gamma = 0 \ ,\end{aligned} \tag{3.31}$$

where since δu is an arbitrary test function, the following relations are deduced

$$\begin{aligned}
\nabla \cdot (\alpha \nabla u) &= 0 \quad \text{on } \Omega \ , \\
\boldsymbol{n} \cdot \alpha \nabla u &= h \quad \text{on } \Gamma_h \ , \\
[\alpha u_{,N}] &= 0 \quad \text{on } \Gamma_D \ , \\
\nabla u^+ \cdot \boldsymbol{n}^+ \equiv u^+_{,N} &= 0 \quad \text{on } \Gamma_F \ , \\
\nabla u^- \cdot \boldsymbol{n}^- \equiv u^-_{,N} &= 0 \quad \text{on } \Gamma_F \ ,
\end{aligned}$$

which are identical to the strong form and its corresponding boundary conditions presented earlier. We note before closing this section that the weak form of any PDE with discontinuous coefficients can be obtained in the same vein as presented above.

3.5 XFEM Applied to Fracture Mechanics

We emphasize that this report is aimed at presenting the fundamentals of the XFEM and its current state of development. It is not our intention to dwell into any particular application. Our main application is on two-fluid flow problems which will be presented in the next chapter. The reason for including a section on the application of the XFEM to crack problems is twofold. First, the development of the XFEM was motivated by fracture mechanics problems and the majority of XFEM applications in the literature has, since then, been very much focused on cracks. Second, the crack tip of a crack affords an interesting example of a physical problem which exhibits neither a weak nor a strong discontinuity. It is often called a singularity in the XFEM literature.

We will first present the strong and weak forms of the governing equations for the displacement field in an elastostatic analysis. Similar to the example given in the previous section, we consider a domain Ω with boundary Γ. The boundary consists of two parts, Γ_h where the traction is prescribed and Γ_u where the displacement is prescribed. Further, we introduce a crack surface Γ_F which is assumed traction free. Γ_F consists of two coincident surfaces Γ_F^- and Γ_F^+. The situation is illustrated in Fig. 17.

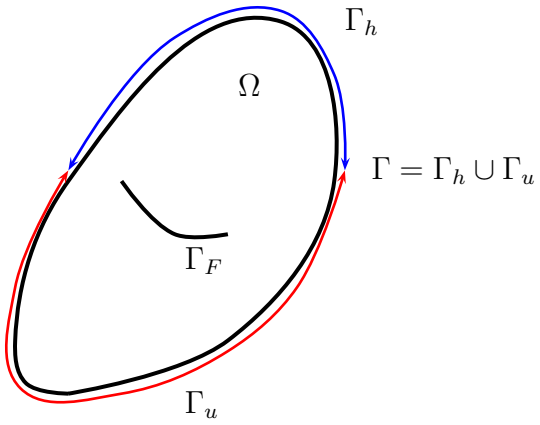

Figure 17: Domain, Ω containing a traction-free crack surface, Γ_F with traction and displacement boundary conditions being prescribed on Γ_h and Γ_u, respectively.

The strong form of the equilibrium equation with corresponding boundary conditions are

$$\sigma_{ji,j} + b_i = 0 \quad \text{in} \quad \Omega \ , \tag{3.32}$$

$$n_j \sigma_{ji} = \bar{t}_i \quad \text{on} \quad \Gamma_h \ , \tag{3.33}$$

$$n_j \sigma_{ji} = 0 \quad \text{on} \quad \Gamma_F^+ \ , \tag{3.34}$$

$$n_j \sigma_{ji} = 0 \quad \text{on} \quad \Gamma_F^- \ , \tag{3.35}$$

$$u_i = \bar{u}_i \quad \text{on} \quad \Gamma_u \ , \tag{3.36}$$

where $\bar{t}_i$ is the prescribed traction on Γ_h, $\bar{u}_i$ is the prescribed displacement on Γ_u, σ_{ji} is the Cauchy stress tensor, n_i is the unit outward normal vector and b_i is the body force vector.

Since we consider only small deformations in linear elasticity, the strain-displacement relation can be written as

$$\epsilon_{ij} = \frac{1}{2}(u_{i,j} + u_{j,i}) \ , \tag{3.37}$$

where ϵ_{ij} is the linear strain tensor. The constitutive relation is given by

$$\sigma_{ij} = C_{ijkl}\epsilon_{kl} \ , \tag{3.38}$$

where C_{ijkl} is the fourth-order Hooke tensor. Next, we define the trial and test spaces as

$$\mathcal{U} = \{u_i \mid u_i \in \mathcal{C}^0,\ u_i = \bar{u}_i \text{ on } \Gamma_u,\ u_i \text{ discontinuous on } \Gamma_F\}\ , \tag{3.39}$$

$$\mathcal{U}_0 = \{\delta u_i \mid \delta u_i \in \mathcal{C}^0,\ \delta u_i = 0 \text{ on } \Gamma_u,\ \delta u_i \text{ discontinuous on } \Gamma_F\}\ . \tag{3.40}$$

We can now go through the same procedure as presented in the previous section and eventually arrive at the following weak form: Find $u_i \in \mathcal{U}$ such that

$$\int_\Omega \epsilon_{ij} C_{ijkl} \epsilon_{kl}\, \mathrm{d}\Omega = \int_\Omega b_i \delta u_i\, \mathrm{d}\Omega + \oint_{\Gamma_h} \bar{t}_i \delta u_i\, \mathrm{d}\Gamma, \quad \forall \delta u_i \in \mathcal{U}_0\ . \tag{3.41}$$

We now move on to the geometric description of the crack. Stolarska *et al.* [59] were the first to propose using the level-set method in the XFEM context to describe the geometry of discontinuities. For example, to describe a crack which begins at an edge and ends in the interior, we employ two level-set functions as shown in Fig. 18.

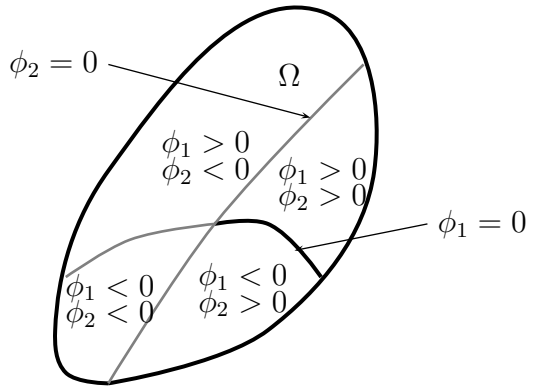

Figure 18: Two level-set functions, ϕ_1 and ϕ_2 are employed to describe an edge crack.

As a crack possesses a strong discontinuity in the displacement field, the Heaviside function is used along the crack path. Also, as singular stresses and strains are found at the crack tip, additional special enrichment functions are employed to represent such singular quantities

at the crack tip. These special enrichment functions are given as,

$$\psi^1(r,\theta) = \sqrt{r}\,\sin\frac{\theta}{2}\ , \tag{3.42}$$

$$\psi^2(r,\theta) = \sqrt{r}\,\sin\frac{\theta}{2}\sin\theta\ , \tag{3.43}$$

$$\psi^3(r,\theta) = \sqrt{r}\,\cos\frac{\theta}{2}\ , \tag{3.44}$$

$$\psi^4(r,\theta) = \sqrt{r}\,\cos\frac{\theta}{2}\sin\theta\ , \tag{3.45}$$

where

$$r = \|\boldsymbol{x} - \boldsymbol{x}^{\text{tip}}\|\ . \tag{3.46}$$

These enrichment functions were first given by Fleming *et.al.* [29] in the context of the Element-Free Galerkin Method (EFG). We note that the angle, θ in (3.42) to (3.45) is defined from $-\pi$ to π (see Fig. 19). Therefore, the function ψ^1 is discontinuous across the crack face whereas the other three functions are continuous. That is, ψ^1 represents the strong discontinuity near the crack tip and the four functions together span the *Westergaard* solution near the tip [12]. The crack tip enrichment functions are shown in Fig. 20.

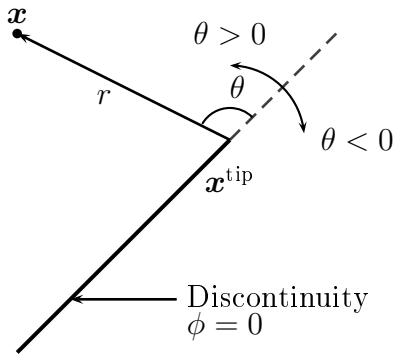

Figure 19: Definition of the polar angle θ for the crack tip enrichment functions.

Based on the enrichment functions presented above, the XFEM approximation takes the

form

$$u^h(\boldsymbol{x}) = \sum_{i\in I} N_i(\boldsymbol{x})\, u_i + \sum_{i\in I_1^*} N_i^*(\boldsymbol{x})\, a_i H(\boldsymbol{x}) + \sum_{j=1}^{4}\sum_{i\in I_2^*} N_i^*(\boldsymbol{x})\, b_i^j \psi^j(\boldsymbol{x}) \quad , \quad (3.47)$$

where $\{\psi^j : j = 1, \ldots, 4\}$ are the crack tip enrichment functions defined in (3.42) to (3.45). One possible arrangement of the nodal subsets, I_1^* and I_2^* is shown in Fig. 21. We see that I_2^* is the set of nodes of the element where the crack tip lies. I_1^* is the set of nodes of the elements completely crossed by the crack and which are *not* in I_2^*. However, Laborde *et al.* [42] demonstrated that in order to achieve optimal convergence rates, the nature of the crack tip singularity dictates that it is necessary to have a tip enrichment area independent of the mesh size. The situation is illustrated in Fig. 22. We see that I_2^* is the set of nodes encompassed by a circle which is at a certain fixed radius from the crack tip. I_1^* is the set of nodes of the elements completely crossed by the crack and which are *not* in I_2^*. However, Laborde *et al.* [42] also noted that the conditioning of the system was negatively affected for the combination of fine mesh resolutions with comparably large radius of the fixed crack tip enrichment area.

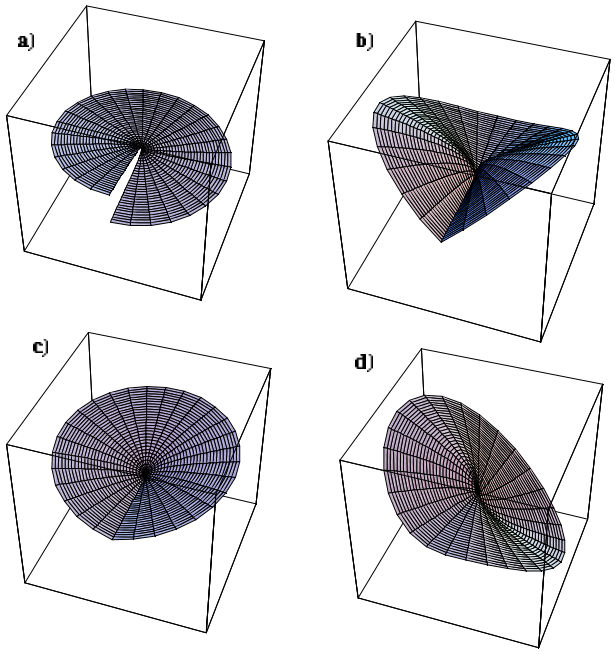

Figure 20: Crack tip enrichment functions: a) ψ^1, b) ψ^2, c) ψ^3, and d) ψ^4.

We note that excellent results have been achieved using the XFEM approximation (3.47) for cracks without special treatment of the blending elements. The most likely reason is that the crack tip enrichment functions approach constant values rapidly away from the singularity so that any parasitic terms introduced in the blending elements can be compensated by the standard FE part of the approximation, just like for the case of the Heaviside enrichment.

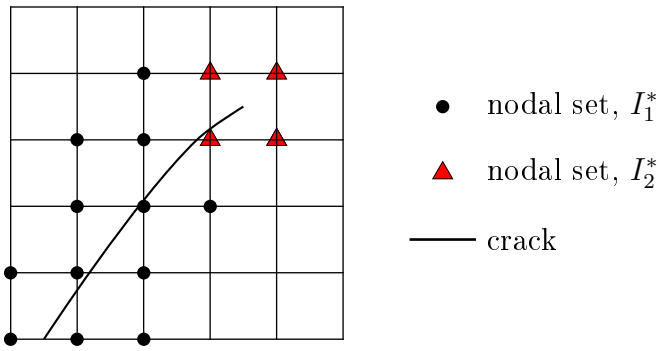

Figure 21: One possible choice for assigning nodal subsets, I_1^* and I_2^* for a crack.

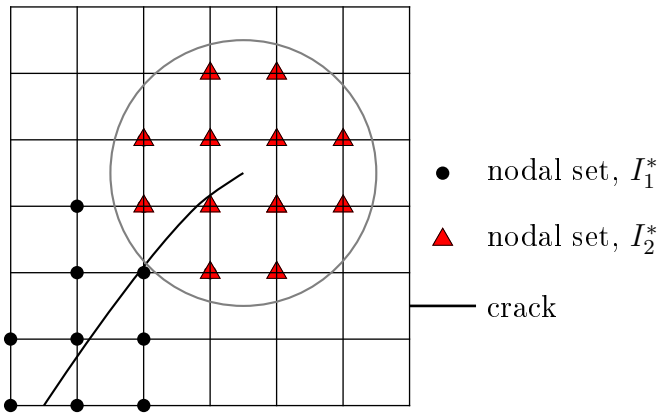

Figure 22: An arrangement of nodal subsets, I_1^* and I_2^* for a crack which is shown to achieve optimal convergence rates. The circle defines a fixed region within which all nodes are enriched with the crack tip enrichments.

The XFEM has been applied to a multitude of physical problems ever since it was first proposed in 1999. Before we close this section, we would like to enumerate a list of XFEM applications with corresponding references in Table 1. For brevity, these applications will not be discussed in detail in this report. Instead, the reader is encouraged to refer to the corresponding literature for more information on specific applications. Finally, we note that the list presented here is by no means exhaustive.

Table 1: List of XFEM applications.

Application	Author(s)
Cracks	Belytschko *et al.* (1999) [12], Moës *et al.* (1999) [48], Daux *et al.* (2000) [25], Sukumar *et al.* (2000) [64], Bechet *et al.* (2005) [11],
Dynamic crack propagation	Stolarska *et al.* (2001) [59], Belytschko *et al.* (2003) [13], Ventura *et al.* (2003) [73], Areias *et al.* (2005) [2, 3]
Cohesive cracks	Zi *et al.* (2003) [79], Asferg *et al.* (2007) [5]
Higher order elements for cracks	Stazi *et al.* (2003) [58], Legay *et al.* (2005) [43], Laborde *et al.* (2005) [42]
Shear band propagation	Areias *et al.* (2006) [4], Song *et al.* (2006) [57]
Dislocations	Ventura *et al.* (2005) [74], Gracie *et al.* (2007) [33]
Solidification	Chessa *et al.* (2002) [22], Dolbow *et al.* (2002) [26], Ji *et al.* (2002) [41]
Voids	Sukumar *et al.* (2001) [63]
Microcracks	Loehnert *et al.* (2007) [44]
Two-fluid flow	Chessa (2003) [17], Chessa *et al.* (2003) [19, 18]
Particulate flow	Wagner *et al.* (2001) [76], Wagner *et al.* (2003) [75]
Boundary layers	Smith *et al.* (2007) [56]
Problems in blending elements	Chessa *et al.* (2003) [23], Gracie *et al.* (2007) [34], Fries (2007) [31]

3.6 Higher-Order Elements for XFEM

It is well-known that in the standard FE approximation, higher-order elements can be employed to improve the accuracy for smooth problems. For physical problems with discontinuities, the XFEM with piecewise linear elements have so far been used with success with optimal convergence rates being reported for many applications (see e.g. [34, 31]). Investigations into the use of higher-order elements in the XFEM context have so far been limited to only stationary problems in structural mechanics [58, 43, 42]. Among these, none has reported achieving optimal higher-order convergence rates for curved discontinuities.

The first investigation into the use of higher-order elements in the XFEM was done by Stazi *et al.* [58] who considered curved cracks and used piecewise quadratic finite elements for the standard FE part and piecewise linear elements for the enriched part of the XFEM approximation

$$\begin{aligned} u^h(\boldsymbol{x}) &= \sum_{i\in I} N_i(\boldsymbol{x})\, u_i + \sum_{i\in I_1^*} N_i^*(\boldsymbol{x})\, a_i \Big(H\big(\phi(\boldsymbol{x})\big) - H\big(\phi(\boldsymbol{x}_i)\big)\Big) \\ &\quad + \sum_{j=1}^{4} \sum_{i\in I_2^*} N_i^*(\boldsymbol{x})\, b_i^j \big(\psi^j(\boldsymbol{x}) - \psi^j(\boldsymbol{x}_i)\big) \ , \end{aligned} \tag{3.48}$$

where $\phi(\boldsymbol{x})$ is the level-set function and $\{\psi^j : j = 1, \ldots, 4\}$ are the crack tip enrichment functions already defined in (3.42) to (3.45). $N_i(\boldsymbol{x})$ are quadratic FE shape functions whereas $N_i^*(\boldsymbol{x})$ are linear FE shape functions. No justification was given for using only linear approximation for the PU functions. Due to the use of quadratic shape functions $N_i(\boldsymbol{x})$, accuracy was improved. However, they did not achieve optimal higher-order convergence rates and blamed it on the presence of the singularity at the crack tip.

Legay *et al.* [43] applied higher-order spectral elements to problems with both weak and strong discontinuities. Their XFEM approximation for a weak discontinuity is given as

$$u^h(\boldsymbol{x}) = \sum_{i\in I} N_i^P(\boldsymbol{x})\, u_i + \sum_{i\in I_1^*} N_i^{P-1}(\boldsymbol{x})\, a_i \big(|\phi(\boldsymbol{x})| - |\phi(\boldsymbol{x}_i)| \big) \ , \tag{3.49}$$

where $\phi(\boldsymbol{x})$ is the level-set function. It is noted that the PU functions $N_i^{P-1}(\boldsymbol{x})$ are spectral functions one order lower than the spectral FE shape functions $N_i^P(\boldsymbol{x})$. This is done to eliminate any problems in blending elements for the abs-enrichment employed for the weak

discontinuity (see Section 3.3). For a strong discontinuity, they used

$$u^h(\boldsymbol{x}) = \sum_{i\in I} N_i^P(\boldsymbol{x})\, u_i + \sum_{i\in I_1^*} N_i^1(\boldsymbol{x})\, a_i \Big(H\big(\phi(\boldsymbol{x})\big) - H\big(\phi(\boldsymbol{x}_i)\big)\Big) \quad , \tag{3.50}$$

where it is noted that the PU functions $N_i^1(\boldsymbol{x})$ are now linear shape functions as opposed to the $N_i^{P-1}(\boldsymbol{x})$ functions used in (3.49). The use of linear PU functions was not explicitly justified but one can reasonably surmise that the purpose was to keep the number of degrees-of-freedom in the enriched part of the approximation to a minimum. They applied the approximation (3.49) to two problems, the first being a manufactured bimaterial problem with a straight, weak discontinuity; the second being a circular inclusion problem with a curved, weak discontinuity. Results for problems with strong discontinuities were not presented. Optimal higher-order convergence rate was reported for the first problem with the $N_i^{P-1}(\boldsymbol{x})$ PU functions. For the second problem, however, $N_i^1(\boldsymbol{x})$ PU functions were found to give better results than $N_i^{P-1}(\boldsymbol{x})$ PU functions originally intended for (3.49), but neither recovered the supposedly optimal higher-order convergence rates. The authors attributed this suboptimality to the quadrature procedure, even though 6-node curved triangular subcells were employed.

Laborde *et al.* [42] studied *straight* cracks and proposed a number of improvements to achieve optimal convergence rates. First, contrary to the works of Stazi *et al.* and Legay *et al.*, Laborde *et al.* argued that in order to have an optimal convergence rate, the PU functions for a strong discontinuity have to be of the same degree as the shape functions $N_i^P(\boldsymbol{x})$ for the standard FE part of the XFEM approximation. They argued that if linear PU functions are used for the strong discontinuity, the displacement jump will be represented as a piecewise linear function along the crack and this is incompatible with the higher-order FE shape functions $N_i^P(\boldsymbol{x})$ being used. Next, they employed a crack tip enrichment area independent of the mesh size (see Section 3.5). However, optimal convergence rates were not achieved and they attributed this to the bad conditioning of the resulting linear system due to the increased degrees-of-freedom used for the crack-tip enrichment. To circumvent this problem, they proposed what they called the *Degrees of Freedom Gathering* for the crack tip enrichment functions. We will explain in detail the fundamental concepts behind this novel idea in the following paragraphs.

As the enriched circular disk around the crack tip (see Fig. 22) encompasses more nodes than is normally the case, the number of degrees-of-freedom is increased markedly. Laborde *et al.* realized that in this case of a crack tip enrichment, the PU functions merely provide

a window to localize the global enrichment functions and are not needed to provide enough degrees-of-freedom to the enrichment functions since they already span the *Westergaard* solution near the tip. Therefore, it is possible to revert to the Global-Local approach (see (3.2)) to fully realize the crack tip solution. We note that this method incurs only one additional degree-of-freedom for each global enrichment function. We also mentioned in Section 3.2 that in order to preserve the spareness property in the Global-Local method, we can localize the global enrichment function by setting its values to zero in those parts of the domain where it is not needed. Laborde *et al.* realized this by utilizing a ramp function and multiplying it with the crack-tip enrichment functions. The ramp function is equal to 1.0 within the enriched disk around the crack tip and decreases linearly to zero over the blending elements. They proposed the final approximation as

$$u^h(\boldsymbol{x}) = \sum_{i\in I} N_i(\boldsymbol{x})\, u_i + \sum_{i\in I_1^*} N_i(\boldsymbol{x})\, a_i H\big(\phi(\boldsymbol{x})\big) + \sum_{j=1}^{4} b^j T_R(\boldsymbol{x})\psi^j(\boldsymbol{x}) \quad , \tag{3.51}$$

where the truncation function is defined as

$$T_R(\boldsymbol{x}) = \sum_{i\in I_R} N_i(\boldsymbol{x}) \quad , \tag{3.52}$$

where I_R is the set of nodes within the enriched disk around the crack tip. We see immediately that each crack tip enrichment function adds only one additional degree-of-freedom and the crack tip solution can be represented using only four additional unknowns compared to the previous case when each enriched node within the disk already introduces 4 unknowns.

We remark that the above procedure of multiplying the global enrichment function with a ramp function is similar to that employed by Fries [31] in the Corrected-XFEM procedure. However, the motivations were different. In Laborde *et al.* [42], the motivation was to reduce the large number of unknowns by reverting to the Global-Local approach and using a ramp function to localize the global enrichment function. This is possible since the enrichment functions span the exact solution and the use of the PU functions is gratuitous. In Fries [31], the motivation was to get rid of problems in blending elements from the outset by localizing the global enrichment function. Also, the PU functions are still retained in the enriched part of the approximation (see Section 3.3).

It should be noted that the Heaviside and the crack tip enrichment functions normally do

not lead to problems with the blending elements. However, in realizing (3.51) using the ramp function, (3.52), Laborde *et al.* have inadvertently introduced unwanted parasitic terms in the blending region which now cannot be compensated by the standard FE part of the approximation. The ideal approach is to localize the crack tip enrichment functions without using a ramp function as in the Local PUM approach proposed in Section 3.3. Nevertheless, they went ahead to propose another novel approach to solve the blending problem. The method is very similar to the DG-XFEM method (see Section 3.3). In this method, the domain is decomposed into two overlapping subdomains with one domain containing the crack tip. The PU functions over the two overlapping domains build a complete partition-of-unity over the entire domain. Enrichments are applied over the separate domains but not over the entire domain. As a result, the enrichment is local but there is no need for blending elements. This method is motivated by the realization that the transition layer does not affect the solution and a transition layer with a vanishing width will effectively eliminate the blending problem. Optimal convergence rates were then achieved after implementing this procedure.

We conclude this section by summarizing pertinent points from the above paragraphs. We first note that the approximation (3.51) is the first instance where the XFEM is coupled with the Global-Local method successfully. This is possible since the singularity is analytically known and is spanned by the crack tip enrichment functions, (3.42) to (3.45). In general, if the singularity is not known analytically, one should revert to the usual XFEM approximation. Second, it is still not clear if PU functions of order *one* can be used to achieve optimal convergence rates for higher-order approximations for strong discontinuities. So far, optimal higher-order convergence rates have only been reported for PU functions with the *same* order as that of the standard FE shape functions for strong discontinuities [42]. Finally, for curved discontinuities, there has hitherto been no literature reporting on optimal higher-order convergence rates being achieved.

4 Two-Fluid Flows

Fluid flows with free moving interfaces (or surfaces) encompass a myraid of physical phenomena and industrial processes such as bubbly flows found in bubble column chemical reactors, ocean waves, propulsion of liquid-metal jets and liquid films in coating and drying processes. These phenomena are collectively known as two-fluid flows. The purpose of numerical modelling applied to two-fluid flows is to provide insight into physical processes of which the time and length scales are so small that reliable experimental observations are either too expensive or impossible to make.

In modelling two-fluid flows, several intrinsic difficulties exist. First, jumps in the fluid density and viscosity across the interface need to be accounted for to satisfy the momentum balance in the vicinity of the interface. Second, as surface tension effects play an important role in the interface dynamics, the modelling of the surface tension should be based on physically sound principles so that it can be correctly incorporated into the governing equations.

In this report, we shall assume that a sharp-interface (zero interfacial thickness) exists between the two fluids. This means that the density and viscosity have a jump discontinuity at the interface (see e.g. Batchelor [10]). We will also assume that the interface has a surface tension and that there is no mass transfer through the interface (i.e. the interface is impermeable). Finally, we assume that there are no surfactants present in the fluids (hence no species transport along the interface). Under such conditions we do not have to consider the variations of surface tension coefficient in a direction tangential to the interface direction. In the next section, we will derive the expression for the surface tension to be used in subsequent sections.

4.1 Surface Tension

We shall now derive the expression for the surface tension on an interface separating two fluids. Our objective is to derive the net surface force per unit area $\boldsymbol{f}_s$ on an element on the surface, S. Our account follows closely that of Brackbill *et al.* [15]. The situation is shown in Fig. 23. We consider an element of area $\boldsymbol{\Delta A} = \hat{\boldsymbol{n}}\Delta A$ about the point $\boldsymbol{x}_s$ on S which is enclosed by a curve C having elemental arc length ds. The surface force exerted on the material in ΔA by the material outside ΔA across the elemental line element $\boldsymbol{ds}$ is equal to $\gamma\hat{\boldsymbol{t}}ds$, where $\hat{\boldsymbol{t}}$ is the unit tangent vector to S which is perpendicular to arc length

vector γ is the surface tension coefficient and $\boldsymbol{ds}$ (i.e. $\hat{\boldsymbol{t}}ds = \boldsymbol{ds} \times \hat{\boldsymbol{n}}$). The net surface force on the element ΔA is then found by

$$\begin{aligned} \boldsymbol{f}_s \Delta A &= \oint_C \gamma \hat{\boldsymbol{t}} ds \ , \\ &= \oint_C \left(\boldsymbol{ds} \times \gamma \hat{\boldsymbol{n}} \right) \ . \end{aligned} \tag{4.1}$$

Using Stokes Theorem to convert the contour integral to a surface integral, we obtain

$$\begin{aligned} \boldsymbol{f}_s \Delta A &= -\oint_{\Delta A} \left((\nabla \times \gamma \hat{\boldsymbol{n}}) \times \boldsymbol{dA} \right) \ , \\ &= \oint_{\Delta A} \left(dA (\hat{\boldsymbol{n}} \times \nabla) \times \gamma \hat{\boldsymbol{n}} \right) \ . \end{aligned} \tag{4.2}$$

In the limit when $\Delta A \to 0$, we have

$$\boldsymbol{f}_s \Delta A = \Delta A \big((\hat{\boldsymbol{n}} \times \nabla) \times \gamma \hat{\boldsymbol{n}} \big) \ , \tag{4.3}$$

where we can immediately deduce the relation

$$\boldsymbol{f}_s(\boldsymbol{x}_s) = (\hat{\boldsymbol{n}} \times \nabla) \times \gamma \hat{\boldsymbol{n}} \ . \tag{4.4}$$

Further evaluation of (4.4) leads to

$$\begin{aligned} \boldsymbol{f}_s(\boldsymbol{x}_s) &= (\hat{\boldsymbol{n}} \times \nabla) \times \gamma \hat{\boldsymbol{n}} \\ &= \varepsilon_{klm} \left(\varepsilon_{ijk} n_i \frac{\partial}{\partial x_j} \right) \gamma n_l \\ &= \varepsilon_{klm} \left(\varepsilon_{ijk} n_i \frac{\partial \gamma}{\partial x_j} \right) n_l + \gamma \varepsilon_{klm} \left(\varepsilon_{ijk} n_i \frac{\partial}{\partial x_j} \right) n_l \\ &= (\hat{\boldsymbol{n}} \times \nabla \gamma) \times \hat{\boldsymbol{n}} + \gamma [(\hat{\boldsymbol{n}} \times \nabla) \times \hat{\boldsymbol{n}}] \ . \end{aligned} \tag{4.5}$$

We note that the differential operator ∇ can be decomposed into its tangential and normal components, $\nabla = \nabla_s + \nabla_n$ where $\nabla_n = \hat{\boldsymbol{n}}(\hat{\boldsymbol{n}} \cdot \nabla)$ so that

$$\hat{\boldsymbol{n}} \times \nabla = \hat{\boldsymbol{n}} \times (\nabla_s + \nabla_n) = \hat{\boldsymbol{n}} \times \nabla_s \ , \tag{4.6}$$

since $\hat{\boldsymbol{n}} \times \nabla_n = 0$. Furthermore, from the well-known identity, $(\boldsymbol{b} \times \boldsymbol{c}) \times \boldsymbol{a} = \boldsymbol{c}(\boldsymbol{a} \cdot \boldsymbol{b}) - \boldsymbol{b}(\boldsymbol{a} \cdot \boldsymbol{c})$,

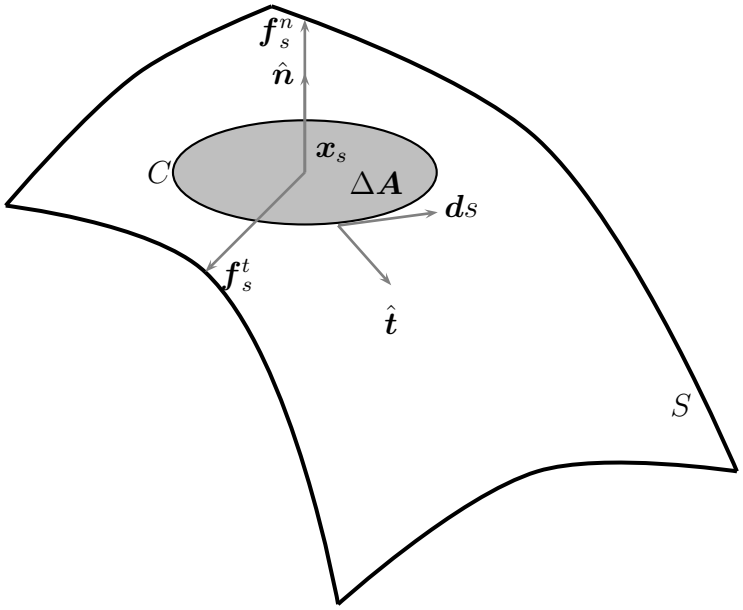

Figure 23: The surface S represents an interface separating two fluids in three dimensions. The tangential component, $\boldsymbol{f}_s^t$ and normal component, $\boldsymbol{f}_s^n$ of the force on the surface element, ΔA due to surface tension on its perimeter C are found by summing the tensile force elements $\gamma \hat{\boldsymbol{t}} ds = \gamma \boldsymbol{ds} \times \hat{\boldsymbol{n}}$ along C.

we deduce

$$(\hat{\boldsymbol{n}} \times \nabla_s) \times \hat{\boldsymbol{n}} = \nabla_s(\hat{\boldsymbol{n}} \cdot \hat{\boldsymbol{n}}) - \hat{\boldsymbol{n}}(\nabla_s \cdot \hat{\boldsymbol{n}}) = -\hat{\boldsymbol{n}}(\nabla_s \cdot \hat{\boldsymbol{n}}) \ , \tag{4.7}$$

$$(\hat{\boldsymbol{n}} \times \nabla\gamma) \times \hat{\boldsymbol{n}} = \nabla\gamma - \hat{\boldsymbol{n}}(\hat{\boldsymbol{n}} \cdot \nabla)\gamma = \nabla_s\gamma \ , \tag{4.8}$$

whereupon substition into (4.5) gives,

$$\boldsymbol{f}_s(\boldsymbol{x}_s) = -\hat{\boldsymbol{n}}\gamma(\nabla_s \cdot \hat{\boldsymbol{n}}) + \nabla_s\sigma \ , \tag{4.9}$$

from which we can immediately identify

$$\boldsymbol{f}_s^n(\boldsymbol{x}_s) = -\hat{\boldsymbol{n}}\gamma(\nabla_s \cdot \hat{\boldsymbol{n}}) \tag{4.10}$$

as the normal component of the surface force and

$$\boldsymbol{f}_s^t(\boldsymbol{x}_s) = \nabla_s\gamma \tag{4.11}$$

as the tangential component of the surface force. The mean curvature at a certain point on the surface, defined as $H = \frac{1}{2}\left(\frac{1}{R_1} + \frac{1}{R_2}\right)$ where R_1 and R_2 are the principal radii of

curvature at the point on the surface, can also be expressed as [15]

$$H = -\frac{1}{2}(\nabla_s \cdot \hat{\boldsymbol{n}}) \ . \tag{4.12}$$

Taking (4.12) into account, (4.10) can then be written as

$$\boldsymbol{f}_s^n(\boldsymbol{x}_s) \ = \ 2H\gamma\hat{\boldsymbol{n}} \ . \tag{4.13}$$

As we have assumed that there is no variation of the surface tension coefficient, γ tangential to the interface, $\boldsymbol{f}_s^t(\boldsymbol{x}_s)$ in (4.11) should vanish. Therefore, the net surface force per unit area from (4.9) is

$$\boldsymbol{f}_s(\boldsymbol{x}_s) \ = \ \kappa\gamma\hat{\boldsymbol{n}} \ , \tag{4.14}$$

where $\kappa = 2H$ has been used.

4.2 Governing Equations in Strong and Weak Forms

In this section, we first present the governing equations in strong form and consequently derive the corresponding weak form. As the FE discretization is based on variational formulation of the problem, it naturally incorporates any discontinuous material coefficients and singular interface-concentrated forces. Further, the use of an FE approximation permits us to localize the interface precisely, without introducing any artificial parameters like interface thickness.

The geometrical situation is depicted in Fig. 24. We consider a d-dimensional domain $\Omega \subset \mathbb{R}^d$ with the boundary $\Gamma = \partial\Omega$. The boundary Γ is decomposed into the Dirichlet and Neumann boundary, $\Gamma_{\boldsymbol{u}}$ and $\Gamma_{\boldsymbol{h}}$, respectively, such that $\Gamma_{\boldsymbol{u}} \cup \Gamma_{\boldsymbol{h}} = \Gamma$ and $\Gamma_{\boldsymbol{u}} \cap \Gamma_{\boldsymbol{h}} = \emptyset$. The normal vector on Γ is denoted $\boldsymbol{n}$. The domain Ω contains two different, immiscible incompressible Newtonian fluids in Ω_1 and Ω_2, respectively, so that $\Omega = \Omega_1 \cup \Omega_2$. We consider Ω to be a time-independent, closed container whereas $\Omega_1(t)$ and $\Omega_2(t)$ change in time. The (moving) interface between the two fluids is denoted Γ_{d}. $\hat{\boldsymbol{n}}$ is the normal vector on Γ_{d} and points from Ω_1 to Ω_2.

The governing equations are now given in strong form, see e.g. [32, 65, 24]. Let $\boldsymbol{u}(\boldsymbol{x}, t)$ be the velocities and $p(\boldsymbol{x}, t)$ the pressure; ϱ_i and μ_i with $i = (1, 2)$ are the density and dynamic viscosity of the two fluids, respectively; $\boldsymbol{f}$ are volumetric forces such as gravity.

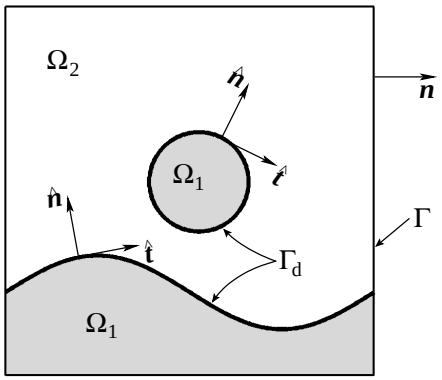

Figure 24: The two fluids in Ω_1 and Ω_2, separated by the interface Γ_d (reproduced from Fries [30]).

The fluids inside $\Omega_i \times (0, t_{\text{end}})$, $i = (1, 2)$, are modeled by the instationary, incompressible Navier-Stokes equations in velocity-pressure formulation

$$\varrho_i \Big(\frac{\partial \boldsymbol{u}}{\partial t} + \boldsymbol{u} \cdot \nabla \boldsymbol{u} \Big) - \nabla \cdot \boldsymbol{\sigma} = \varrho_i \boldsymbol{f}, \tag{4.15}$$

$$\nabla \cdot \boldsymbol{u} = 0. \tag{4.16}$$

The stress tensor $\boldsymbol{\sigma}$ of the Newtonian fluids is given as

$$\boldsymbol{\sigma}(\boldsymbol{u}, p) = -p\mathbf{I} + 2\mu_i \boldsymbol{\varepsilon}(\boldsymbol{u}), \text{ with } \boldsymbol{\varepsilon}(\boldsymbol{u}) = \frac{1}{2}\big(\nabla \boldsymbol{u} + (\nabla \boldsymbol{u})^{\mathrm{T}}\big), \tag{4.17}$$

where $\mathbf{I}$ is the identity tensor. Dirichlet and Neumann boundary conditions on the outer boundary of Ω are

$$\boldsymbol{u} = \hat{\boldsymbol{u}} \quad \text{on } \Gamma_{\boldsymbol{u}} \times (0, t_{\text{end}}), \tag{4.18}$$

$$\boldsymbol{\sigma} \cdot \boldsymbol{n} = \hat{\boldsymbol{h}} \quad \text{on } \Gamma_{\boldsymbol{h}} \times (0, t_{\text{end}}), \tag{4.19}$$

where $\hat{\boldsymbol{u}}$ and $\hat{\boldsymbol{h}}$ are prescribed velocities and stresses. The following conditions typically apply at the interface

$$[\boldsymbol{u}]_{\Gamma_d} = \mathbf{0} \quad \text{on } \Gamma_d \times (0, t_{\text{end}}), \tag{4.20}$$

$$-[\boldsymbol{\sigma}]_{\Gamma_d} \cdot \hat{\boldsymbol{n}} = \gamma \kappa \hat{\boldsymbol{n}} \quad \text{on } \Gamma_d \times (0, t_{\text{end}}). \tag{4.21}$$

Here, $[f]_{\Gamma_\mathrm{d}}$ is the jump of property f across the interface Γ_d, γ is the surface tension coefficient (material parameter) and κ is the curvature of Γ_d. As an initial condition, a divergence-free velocity field $\hat{\boldsymbol{u}}_0$ is specified over Ω,

$$\boldsymbol{u}(\boldsymbol{x},0) = \hat{\boldsymbol{u}}_0(\boldsymbol{x}) \quad \text{in } \Omega \text{ at } t = 0. \tag{4.22}$$

The situation at the interface Γ_d is considered in more detail. The density and viscosity fields

$$\varrho(\boldsymbol{x},t) = \begin{cases} \varrho_1 & \forall \boldsymbol{x} \in \Omega_1(t), \\ \varrho_2 & \forall \boldsymbol{x} \in \Omega_2(t). \end{cases} \qquad \mu(\boldsymbol{x},t) = \begin{cases} \mu_1 & \forall \boldsymbol{x} \in \Omega_1(t), \\ \mu_2 & \forall \boldsymbol{x} \in \Omega_2(t). \end{cases} \tag{4.23}$$

change discontinuously at Γ_d. As a consequence, also the state variables such as the velocities and pressure fields involve discontinuities at the interface. Discontinuities may be classified into strong or weak. In the case of strong discontinuities, a jump and a change in the gradient is present in the field. For weak discontinuities there is only a kink in the field, i.e. the field is continuous with a discontinuous gradient.

The interface condition (4.20) states that the velocities are continuous across Γ_d, or, in other words, that the jump in the velocity field is zero. The second interface condition (4.21), states that the surface tension balances the jump of the normal stress at the interface. As a consequence of (4.15)-(4.16) and (4.20)-(4.21), the velocity fields $\boldsymbol{u}(\boldsymbol{x},t)$ are weakly discontinuous across Γ_d, whereas the pressure field $p(\boldsymbol{x},t)$ has a strong discontinuity at the interface. In the case that no surface tension is considered, $\gamma = 0$ and the jump in the pressure field vanishes and $p(\boldsymbol{x},t)$ has a kink at Γ_d.

We will now proceed to derive the weak form. We first define the trial and test spaces, $\mathcal{S}^h$ and $\mathcal{V}^h$ for the velocities, $\boldsymbol{u}$ and pressure, p as

$$\mathcal{S}_{\boldsymbol{u}}^h = \left\{ \boldsymbol{u}^h \middle| \, \boldsymbol{u}^h \in \left(\mathcal{H}^{1h}\right)^d, \, \boldsymbol{u}^h = \hat{\boldsymbol{u}}^h \text{ on } \Gamma_{\boldsymbol{u}} \right\}, \tag{4.24}$$

$$\mathcal{V}_{\boldsymbol{u}}^h = \left\{ \boldsymbol{w}^h \middle| \, \boldsymbol{w}^h \in \left(\mathcal{H}^{1h}\right)^d, \, \boldsymbol{w}^h = \boldsymbol{0} \text{ on } \Gamma_{\boldsymbol{u}} \right\}, \tag{4.25}$$

$$\mathcal{S}_p^h = \mathcal{V}_p^h = \left\{ q^h \middle| \, q^h \in \mathcal{H}^{1h} \right\}, \tag{4.26}$$

where $\mathcal{H}^{1h} \subseteq \mathcal{H}^1$ is a finite dimensional *Sobolev* space consisting of the FE shape functions $\{N_i\}$; either abs- and/or sign-enrichment is used for the construction of the velocity and pressure shape functions. The space $\mathcal{H}^1$ is the set of functions which are, together with their

first derivatives, square-integrable in Ω. The derivation of the weak form in the following paragraphs is similar to that presented in Section 3.4. We start off with the strong form of the momentum equation (4.15) in tensor notation

$$\varrho_k \left(\frac{\partial u_i}{\partial t} + u_j \frac{\partial u_i}{\partial x_j} \right) = \frac{\partial \sigma_{ij}}{\partial x_j} + \varrho_k f_i \ , \tag{4.27}$$

where ϱ_k with $k = (1, 2)$ is the density of the two fluids. We now multiply (4.27) by the test function, w_i and integrate over the entire domain, Ω

$$\int_\Omega w_i \varrho_k \left(\frac{\partial u_i}{\partial t} + u_j \frac{\partial u_i}{\partial x_j} \right) \mathrm{d}\Omega = \int_\Omega w_i \frac{\partial \sigma_{ij}}{\partial x_j} \mathrm{d}\Omega + \int_\Omega \varrho_k w_i f_i \, \mathrm{d}\Omega \ . \tag{4.28}$$

The first term on the RHS of (4.28) can be further evaluated as

$$\begin{aligned}
\int_\Omega w_i \frac{\partial \sigma_{ij}}{\partial x_j} \mathrm{d}\Omega &= \int_\Omega \left[\frac{\partial}{\partial x_j} (w_i \sigma_{ij}) - \sigma_{ij} \frac{\partial w_i}{\partial x_j} \right] \mathrm{d}\Omega \ , && (4.29) \\
&= \oint_{\Gamma_u \bigcup \Gamma_h \bigcup \Gamma_d} w_i \sigma_{ij} n_j \, \mathrm{d}\Gamma - \int_\Omega \sigma_{ij} \frac{\partial w_i}{\partial x_j} \mathrm{d}\Omega \ , && (4.30) \\
&= \oint_{\Gamma_h} w_i \hat{h}_i \, \mathrm{d}\Gamma + \oint_{\Gamma_d^+} w_i (\sigma_{ij} n_j)^+ \, \mathrm{d}\Gamma + \oint_{\Gamma_d^-} w_i (\sigma_{ij} n_j)^- \, \mathrm{d}\Gamma \\
&\quad - \int_\Omega \sigma_{ij} \frac{\partial w_i}{\partial x_j} \mathrm{d}\Omega \ , && (4.31) \\
&= \oint_{\Gamma_h} w_i \hat{h}_i \, \mathrm{d}\Gamma + \oint_{\Gamma_d} w_i \hat{n}_j \left(\sigma_{ij}^+ + \sigma_{ij}^- \right) \mathrm{d}\Gamma - \int_\Omega \sigma_{ij} \frac{\partial w_i}{\partial x_j} \mathrm{d}\Omega \ , && (4.32) \\
&= \oint_{\Gamma_h} w_i \hat{h}_i \, \mathrm{d}\Gamma + \oint_{\Gamma_d} \gamma \kappa w_i \hat{n}_i \, \mathrm{d}\Gamma - \int_\Omega \sigma_{ij} \frac{\partial w_i}{\partial x_j} \mathrm{d}\Omega \ , && (4.33)
\end{aligned}$$

where the Gauss theorem has been used from (4.29) to (4.30), the definition of the test space $\mathcal{V}_{\boldsymbol{u}}^h$ has been used from (4.30) to (4.31), the interface condition (4.21) has been used from (4.32) to (4.33), $\hat{n}_i = n_i^+$ is the unit normal vector pointing from Ω_1 to Ω_2 and $\Gamma_d = \Gamma_d^+$. Substituting (4.33) into (4.28), we obtain

$$\begin{aligned}
\int_\Omega w_i \varrho_k \left(\frac{\partial u_i}{\partial t} + u_j \frac{\partial u_i}{\partial x_j} \right) \mathrm{d}\Omega + \int_\Omega \sigma_{ij} \frac{\partial w_i}{\partial x_j} \mathrm{d}\Omega - \oint_{\Gamma_h} w_i \hat{h}_i \, \mathrm{d}\Gamma \\
= \int_\Omega \varrho_k w_i f_i \, \mathrm{d}\Omega + \oint_{\Gamma_d} \gamma \kappa w_i \hat{n}_i \, \mathrm{d}\Gamma \ .
\end{aligned} \tag{4.34}$$

The weak form of the continuity equation is found by multiplying (4.16) by the test func-

tion, q_i and integrating over the entire domain, Ω

$$\int_\Omega q_i \frac{\partial u_j}{\partial x_j}\,\mathrm{d}\Omega = 0 \ . \tag{4.35}$$

This is then substituted into (4.34) to obtain

$$\begin{aligned}\int_\Omega w_i \varrho_k \left(\frac{\partial u_i}{\partial t} + u_j \frac{\partial u_i}{\partial x_j}\right)\mathrm{d}\Omega + \int_\Omega \sigma_{ij}\frac{\partial w_i}{\partial x_j}\,\mathrm{d}\Omega - \oint_{\Gamma_h} w_i \hat{h}_i\,\mathrm{d}\Gamma \\ + \int_\Omega q_i \frac{\partial u_j}{\partial x_j}\,\mathrm{d}\Omega = \int_\Omega \varrho_k w_i f_i\,\mathrm{d}\Omega + \oint_{\Gamma_d} \gamma\kappa w_i \hat{n}_i\,\mathrm{d}\Gamma \ .\end{aligned} \tag{4.36}$$

In vector-dyadic notation, the *discretized* weak form can be formulated as: Find $\boldsymbol{u}^h \in \mathcal{S}^h_{\boldsymbol{u}}$ and $p^h \in \mathcal{S}^h_p$ such that $\forall \boldsymbol{w}^h \in \mathcal{V}^h_{\boldsymbol{u}}$ and $\forall q^h \in \mathcal{V}^h_p$,

$$\begin{aligned}\int_\Omega \boldsymbol{w}^h \cdot \varrho_k \left(\frac{\partial \boldsymbol{u}^h}{\partial t} + \boldsymbol{u}^h \cdot \nabla \boldsymbol{u}^h\right) d\Omega + \int_\Omega \boldsymbol{\varepsilon}\left(\boldsymbol{w}^h\right) : \boldsymbol{\sigma}\left(\boldsymbol{u}^h, p^h\right) d\Omega \\ - \oint_{\Gamma_{\boldsymbol{h}}} \boldsymbol{w}^h \cdot \hat{\boldsymbol{h}}\, d\Gamma + \int_\Omega q^h \nabla \cdot \boldsymbol{u}^h d\Omega = \int_\Omega \varrho_k\, \boldsymbol{w}^h \cdot \boldsymbol{f}\, d\Omega + \oint_{\Gamma_d} \gamma\, \kappa\, \boldsymbol{w}^h \cdot \hat{\boldsymbol{n}}\, d\Gamma,\end{aligned} \tag{4.37}$$

with $k = (1, 2)$, and $\boldsymbol{\sigma}$ and $\boldsymbol{\varepsilon}$ are defined in Eq. (4.17). The SUPG/PSPG-stabilized version of the discretized weak form may then be formulated as [69]: Find $\boldsymbol{u}^h \in \mathcal{S}^h_{\boldsymbol{u}}$ and $p^h \in \mathcal{S}^h_p$ such that $\forall \boldsymbol{w}^h \in \mathcal{V}^h_{\boldsymbol{u}}$ and $\forall q^h \in \mathcal{V}^h_p$,

$$\begin{aligned}\int_\Omega \boldsymbol{w}^h \cdot \varrho_k \left(\frac{\partial \boldsymbol{u}^h}{\partial t} + \boldsymbol{u}^h \cdot \nabla \boldsymbol{u}^h\right) d\Omega + \int_\Omega \boldsymbol{\varepsilon}\left(\boldsymbol{w}^h\right) : \boldsymbol{\sigma}\left(\boldsymbol{u}^h, p^h\right) d\Omega \\ - \oint_{\Gamma_{\boldsymbol{h}}} \boldsymbol{w}^h \cdot \hat{\boldsymbol{h}}\, d\Gamma + \int_\Omega q^h \nabla \cdot \boldsymbol{u}^h d\Omega + \sum_{j\in\mathcal{Q}} \int_{\Omega_j^{\mathrm{el}}} \tau_j \left(\boldsymbol{u}^h \cdot \nabla \boldsymbol{w}^h + \frac{1}{\varrho_i}\nabla q^h\right) \\ \cdot \left[\varrho_k \left(\frac{\partial \boldsymbol{u}^h}{\partial t} + \boldsymbol{u}^h \cdot \nabla \boldsymbol{u}^h\right) - \nabla \cdot \boldsymbol{\sigma}\left(\boldsymbol{u}^h, p^h\right)\right] d\Omega = \\ \int_\Omega \varrho_k\, \boldsymbol{w}^h \cdot \boldsymbol{f}\, d\Omega + \oint_{\Gamma_d} \gamma\, \kappa\, \boldsymbol{w}^h \cdot \hat{\boldsymbol{n}}\, d\Gamma,\end{aligned} \tag{4.38}$$

where the additional stabilization terms are found within the summation $\sum_{j\in\mathcal{Q}}$. These terms stabilize oscillations in advection dominated regions and enable equal-order interpolations of the velocities and pressures by circumventing the Babuška-Brezzi condition

[7, 16]. The stabilization parameters τ_j are defined as [53]

$$\tau_j = \left[\left(\frac{2}{\Delta t} \right)^2 + \left(\frac{2 \left\| \boldsymbol{u} \right\|}{h_j} \right)^2 + \left(\frac{4\nu_i}{h_j^2} \right)^2 \right]^{-1/2}, \tag{4.39}$$

where ν_i is the kinematic viscostiy defined as

$$\nu_i = \frac{\mu_i}{\varrho_i}, \tag{4.40}$$

and h_j is computed elementwise as [46]

$$h_j = \sqrt{2} \cdot A_i^{\mathrm{el}} / h_{\mathrm{diag}}, \tag{4.41}$$

with A_j^{el} being the element area and h_{diag} being the larger diagonal distance between the nodes of the quadrilateral element [46].

4.3 Space–Time Formulation

In the XFEM, the enrichment of the approximation depends upon the interface position which moves in time. That is, the enriched shape functions are time–dependent and a standard time–stepping scheme does not take this into account. It is shown in Chessa *et al.* [20] that a space–time finite element formulation is a natural choice for the XFEM. This is because if the discontinuity moves in time, it seems only logical to resolve the discontinuity in time as well as space. In the following paragraphs, we will give a brief overview of the space–time formulation.

We consider a space-time domain, $\Pi = \Omega \times]0, T[$ which is the Cartesian product of the spatial domain, Ω and the temporal domain, $]0, T[$. The domain is then subdivided into m time slabs with the n^{th} time slab being denoted by Π^n defined as

$$\Pi^n = \Omega \times]t^{n-1}, t^n[\ . \tag{4.42}$$

The approximations $\boldsymbol{u}^h(\boldsymbol{x}, t)$ are discontinuous across time slabs, but continuous in the slab. The slab may be discretized in any desired manner and the discretizations need not be contiguous across adjacent slabs. The space–time surface of discontinuity is denoted as Γ_l as shown in Fig. 25.

We note that the space-time formulation is able to resolve the discontinuity in space and time while a semi-discretized approach can only resolve the discontinuity in space, thus leading to more accurate results of the space-time formulation. It was shown in [20] that implicit semi-discrete enriched finite element formulations can be expressed as a degenerate case of the space-time formulation where the interpolation is constant in time. Also, both the semi-discrete approach and space-time formulation project the solutions from the previous time step/slab approximation space to the current approximation space in the L^2 norm. Therefore, any improvement of the space-time formulation can be attributed to the fact that the approximation spaces in the discontinuous space-time formulation can better reproduce the discontinuities in space and time, thereby minimizing the error in the projection. In a subsequent work, Chessa *et al.* [21] used standard semi-discretization methods along the time lines not crossed by the discontinuity and the space-time method only where it is needed in order to optimize the speed of computation.

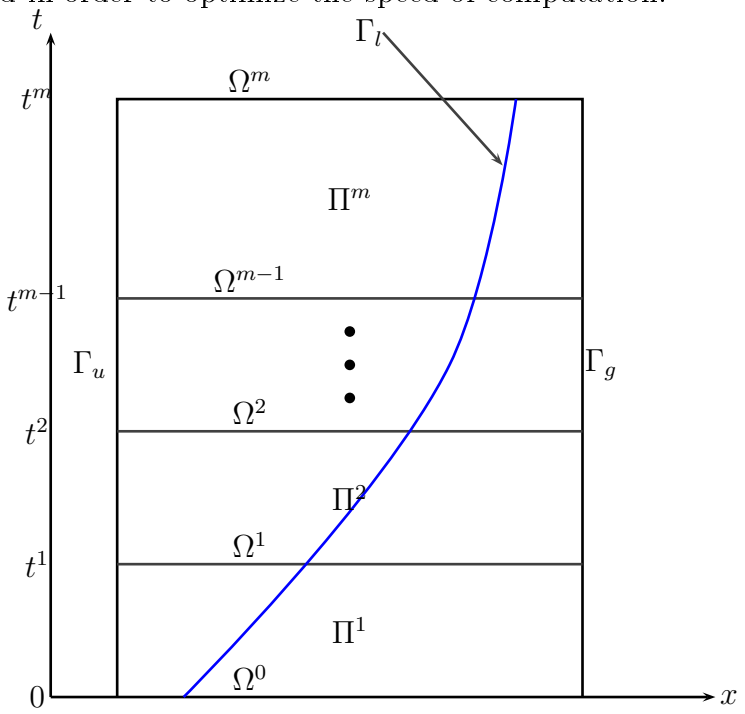

Figure 25: A typical space–time domain, Π; blue curve shows space–time discontinuity.

However, it was argued in Fries [30] that time-stepping methods may also be used as a simplification since time-derivatives of *weakly* discontinuous fields (such as the velocity fields in two-fluid flows) can, in fact, be discretized with very satisfactory results by standard time-stepping schemes.

5 Conclusion

We have given a basic introduction to the fundamentals of the XFEM and its current state of development in this short report. Particular attention has been devoted to the logical development of the XFEM as an offspring of the Partition-of-Unity Method (PUM). This point of view enables us to eliminate any problems in blending elements from the outset by adhering to an admissible localized global enrichment function. We have also illustrated that the XFEM can be coupled with the Global-Local method in problems where the discontinuity is exactly spanned by the enrichment functions alone, thus doing away with the need for additional PU functions and leading to fewer degrees-of-freedom. This has first been realized in the work of Laborde *et al.* [42]. Finally, we have demonstrated how the weak form can be derived from the classical strong form of the governing equations of various physical problems via a standard procedure which utilizes the Gauss theorem to convert a volume integral into a surface integral. The natural boundary conditions on the interface are then recovered as by-products of the procedure.

References

[1] Adalsteinsson, D.; Sethian, J.A.: A Fast Level Set Method for Propagating Interfaces. *J. Comput. Phys.*, **118**, 269 – 286, 1995.

[2] Areias, P.M.A.; Belytschko, T.: Analysis of three-dimensional crack initiation and propagation using the extended finite element method. *Internat. J. Numer. Methods Engrg.*, **63**, 760 – 788, 2005.

[3] Areias, P.M.A.; Belytschko, T.: Non-linear analysis of shells with arbitrary evolving cracks using XFEM. *Internat. J. Numer. Methods Engrg.*, **62**, 384–415, 2005.

[4] Areias, P.M.A.; Belytschko, T.: Two-scale shear band evolution by local partition of unity. *Internat. J. Numer. Methods Engrg.*, **66**, 878 – 910, 2006.

[5] Asferg, J.L.; Poulsen, P.N.; Nielsen, L.O.: A consistent partly cracked XFEM element for cohesive crack growth. *Internat. J. Numer. Methods Engrg.*, **72**, 464–485, 2007.

[6] B. Merriman, J. Bence; Osher, S.: Motion of multiple junctions: A level set approach. *J. Comput. Phys.*, **112**, p. 334, 1994.

[7] Babuška, I.: Error-bounds for finite element method. *Numer. Math.*, **16**, 322 – 333, 1971.

[8] Babuška, I.; Melenk, J.M.: The partition of unity finite element method. Technical Report BN-1185, Institute for Physical Science and Technology, University of Maryland, 1995.

[9] Babuška, I.; Melenk, J.M.: The Partition of Unity Method. *Internat. J. Numer. Methods Engrg.*, **40**, 727 – 758, 1997.

[10] Batchelor, G.K.: *An Introduction to Fluid Dynamics*. Cambridge University Press, Cambridge, 1967.

[11] Béchet, E.; Minnebo, H.; Moës, N.; Burgardt, B.: Improved implementation and robustness study of the X-FEM for stress analysis around cracks. *Internat. J. Numer. Methods Engrg.*, **64**, 1033–1056, 2005.

[12] Belytschko, T.; Black, T.: Elastic Crack Growth in Finite Elements with Minimal Remeshing. *Internat. J. Numer. Methods Engrg.*, **45**, 601 – 620, 1999.

[13] Belytschko, T.; Chean, H.; Xu, J.; Zi, G.: Dynamic Crack Propagation Based on Loss of Hyperbolicity and a New Discontinuous Enrichment. *Internat. J. Numer. Methods Engrg.*, **58**, 1873 – 1905, 2003.

[14] Belytschko, T.; Moës, N.; Usui, S.; Parimi, C.: Arbitrary discontinuities in finite elements. *Internat. J. Numer. Methods Engrg.*, **50**, 993 – 1013, 2001.

[15] Brackbill, J. U.; Kothe, D. B.; Zemach, C.: A continuum method for modeling surface tension. *J. Comput. Phys.*, **100**, 335–354, 1992.

[16] Brezzi, F.: On the existence, uniqueness and approximation of saddle-point problems arising from Lagrange multipliers. *RAIRO Anal. Numér.*, **R-2**, 129 – 151, 1974.

[17] Chessa, J.: *The extended finite element method for two phase and free surface flow.* Dissertation, Northwestern University, 2003.

[18] Chessa, J.; Belytschko, T.: An enriched finite element method and level sets for axisymmetric two-phase flow with surface tension. *Internat. J. Numer. Methods Engrg.*, **58**, 2041 – 2064, 2003.

[19] Chessa, J.; Belytschko, T.: The Extended Finite Element Method for Two-Phase Fluids. *ASME J. Appl. Mech.*, **70**, 10 – 17, 2003.

[20] Chessa, J.; Belytschko, T.: Arbitrary Discontinuities in Space-Time Finite Elements by Level-Sets and X-FEM. *Internat. J. Numer. Methods Engrg.*, **61**, 2595 – 2614, 2004.

[21] Chessa, J.; Belytschko, T.: A local spaceŰtime discontinuous finite element method. *Comp. Methods Appl. Mech. Engrg.*, **195**, 1325 – 1343, 2006.

[22] Chessa, J.; Smolinski, P.; Belytschko, T.: The Extended Finite Element Method (XFEM) for Solidification Problems. *Internat. J. Numer. Methods Engrg.*, **53**, 1959 – 1977, 2002.

[23] Chessa, J.; Wang, H.; Belytschko, T.: On the Construction of Blending Elements for Local Partition of Unity Enriched Finite Elements. *Internat. J. Numer. Methods Engrg.*, **57**, 1015 – 1038, 2003.

[24] Cruchaga, M.; Celentano, D.; Breitkopf, P.; Villon, P.; Rassineux, A.: A front remeshing technique for a Lagrangian description of moving interfaces in two-fluid flows. *Internat. J. Numer. Methods Engrg.*, **66**, 2035 – 2063, 2006.

[25] Daux, C.; Moës, N.; Dolbow, J.E.; Sukumar, N.: Arbitrary Branched and Intersecting Cracks with the Extended Finite Element Method. *Internat. J. Numer. Methods Engrg.*, **48**, 1741 – 1760, 2000.

[26] Dolbow, J.E.; Merle, R.: Solving Thermal and Phase Change Problems with the Extended Finite Element Method. *Comput. Mech.*, **28**, 339 – 350, 2002.

[27] Dolbow, J.E.; Moës, N.; Belytschko, T.: Discontinuous Enrichment in Finite Elements with a Partition of Unity Method. *Internat. J. Numer. Methods Engrg.*, **36**, 235 – 260, 2000.

[28] Duarte, C.A.M.; Oden, J.T.: Hp clouds – a meshless method to solve boundary-value problems. Technical Report 95-05, TICAM, The University of Texas at Austin, 1995.

[29] Fleming, M.; Chu, Y.A.; Moran, B.; Belytschko, T.: Enriched element-free galerkin methods for crack tip fields. *Internat. J. Numer. Methods Engrg.*, **40**, 1483–1504, 1997.

[30] Fries, T. P.: The intrinsic XFEM for two-fluid flows. *Int. J. Numer. Methods Fluids*, accepted.

[31] Fries, T.P.: A corrected XFEM approximation without problems in blending elements. *Internat. J. Numer. Methods Engrg.*, DOI 10.1002/nme.2259, 2007.

[32] Ganesan, S.; Matthies, G.; Tobiska, L.: On spurious velocities in incompressible flow problems with interfaces. *Comp. Methods Appl. Mech. Engrg.*, doi:10.1016/j.cma.2006.08.018, 2006.

[33] Gracie, R.; Ventura, G.; Belytschko, T.: A new fast method for dislocations based on interior discontinuities. *Internat. J. Numer. Methods Engrg.*, **69**, 423–441, 2007.

[34] Gracie, R.; Wang, H.W.; Belytschko, T.: Blending in the extended finite element method by discontinuous Galerkin and assumed strain methods. *Internat. J. Numer. Methods Engrg.*, –, 2007.

[35] Güler, I.; Behr, M.; Tezduyar, T.: Parallel Finite Element Computation of Free-Surface Flows. *Comput. Mech.*, **23**, 117 – 123, 1999.

[36] Harlow, J.H.; Welch, J.E.: Numerical study of large amplitude free surface motion. *Physics of Fluids*, **9**, 842–851, 1966.

[37] Harten, A.; Engquist, B.; Osher, S.; Chakravarthy, S.: Uniformly High- Order Accurate Essentially Non-Oscillatory Schemes III. *J. Comput. Phys.*, **71**, 231 – 303, 1987.

[38] Hirt, C.W.; Nichols, B.D.: Volume of fluid (VOF) method for the dynamics of free boundaries. *J. Comput. Phys.*, **39**, 201 – 225, 1981.

[39] Huerta, A.; Liu, W.K.: Viscous flow with large free surface motion. *Comp. Methods Appl. Mech. Engrg.*, **69**, 277 – 324, 1988.

[40] Hughes, T.J.R.: *The Finite Element Method: Linear Static and Dynamic Finite Element Analysis*. Prentice-Hall, Englewood Cliffs, NJ, 1987.

[41] Ji, H.; Chopp, D.; Dolbow, J.E.: A Hybrid Extended Finite Element/Level Set Method for Modeling Phase Transformations. *Internat. J. Numer. Methods Engrg.*, **54**, 1209 – 1233, 2002.

[42] Laborde, P.; Pommier, J.; Renard, Y.; Salaün, M.: High-order Extended Finite Element Method for Cracked Domains. *Internat. J. Numer. Methods Engrg.*, **64**, 354 – 381, 2005.

[43] Legay, A.; Wang, H. W.; Belytschko, T.: Strong and weak arbitrary discontinuities in spectral finite elements. *Internat. J. Numer. Methods Engrg.*, **64**, 991–1008, 2005.

[44] Loehnert, S.; Belytschko, T.: A multiscale projection method for macro/microcrack simulations. *Internat. J. Numer. Methods Engrg.*, **71**, 1466–1482, 2007.

[45] Melenk, J.M.; Babuška, I.: The Partition of Unity Finite Element Method: Basic Theory and Applications. *Comp. Methods Appl. Mech. Engrg.*, **139**, 289 – 314, 1996.

[46] Mittal, S.: On the performance of high aspect ratio elements for incompressible flows. *Comp. Methods Appl. Mech. Engrg.*, **188**, 269 – 287, 2000.

[47] Moës, N.; Cloirec, M.; Cartaud, P.; Remacle, J.F.: A computational approach to handle complex microstructure geometries. *Comp. Methods Appl. Mech. Engrg.*, **192**, 3163–3177, 2003.

[48] Moës, N.; Dolbow, J.; Belytschko, T.: A finite element method for crack growth without remeshing. *Internat. J. Numer. Methods Engrg.*, **46**, 131 – 150, 1999.

[49] Mote, C.D.: Global-local finite element. *Internat. J. Numer. Methods Engrg.*, **3**, 565 – 574, 1971.

[50] Osher., S.; Sethian, J.: Fronts Propagating with Curvature Dependent Speed: Algorithms Based on Hamilton-Jacobi Formulations. *J. Comput. Phys.*, **79**, 12–49, 1988.

[51] Peng, D.; Merriman, B.; S.Osher; Zhao, H.; Kang, M.: A PDE-based fast local level set method. *J. Comput. Phys.*, **155**, 410–438, 1999.

[52] Peskin, C.: Numerical Analysis of Blood Flow in the Heart. *J. Comput. Phys.*, **25**, 220–252, 1977.

[53] Shakib, F.; Hughes, T.J.R.; Johan, Z.: A new finite element formulation for computational fluid dynamics: X. The compressible Euler and Navier-Stokes equations. *Comp. Methods Appl. Mech. Engrg.*, **89**, 141 – 219, 1991.

[54] Shilov, G.E.: *Elementary Real and Complex Analysis*. Dover, New York, NY, 1996.

[55] Simo, J.C.; Rifai, M.S.: A class of mixed assumed strain methods and the method of incompatible modes. *Internat. J. Numer. Methods Engrg.*, **29**, 1595–1638, 1990.

[56] Smith, B.G.; Vaughan, B.L.; Chopp, D.L.: The extended finite element method for boundary layer problems in biofilm growth. *Comm. App. Math. Comp. Sci.*, **2**, 35–56, 2007.

[57] Song, J.H.; Areias, P.M.A.; Belytschko, T.: A method for dynamic crack and shear band propagating with phantom nodes. *Internat. J. Numer. Methods Engrg.*, **67**, 868–893, 2006.

[58] Stazi, F.L.; Budyn, E.; Chessa, J.; Belytschko, T.: An extended finite element method with higher-order elements for crack problems with curvature. *Comput. Mech.*, **31**, 38 – 48, 2003.

[59] Stolarska, M.; Chopp, D.L.; Moës, N.; Belytschko, T.: Modelling Crack Growth by Level Sets in the Extended Finite Element Method. *Internat. J. Numer. Methods Engrg.*, **51**, 943 – 960, 2001.

[60] Strouboulis, T.; Babuška, I.; Copps, K.: The design and analysis of the generalized finite element method. *Comp. Methods Appl. Mech. Engrg.*, **181**, 43 – 69, 2000.

[61] Strouboulis, T.; Copps, K.; Babuška, I.: The Generalized Finite Element Method: An Example of its Implementation and Illustration of its Performance. *Internat. J. Numer. Methods Engrg.*, **47**, 1401 – 1417, 2000.

[62] Strouboulis, T.; Copps, K.; Babuška, I.: The Generalized Finite Element Method. *Comp. Methods Appl. Mech. Engrg.*, **190**, 4081 – 4193, 2001.

[63] Sukumar, N.; Chopp, D.L.; Moës, N.; Belytschko, T.: Modeling holes and inclusions by level sets in the extended finite-element method. *Comp. Methods Appl. Mech. Engrg.*, **190**, 6183 – 6200, 2001.

[64] Sukumar, N.; Moës, N.; Moran, B.; Belytschko, T.: Extended Finite Element Method for Three-Dimensional Crack Modeling. *Internat. J. Numer. Methods Engrg.*, **48**, 1549 – 1570, 2000.

[65] Sussman, M.; Smereka, P.; Osher, S.: A level set approach for computing solutions to incompressible two-phase flow. *J. Comput. Phys.*, **114**, 146 – 159, 1994.

[66] Sussmann, M.; Fatemi, E.: An Efficient Interface-Preserving Level Set Redistancing Algorithm and Its Application to Interfacial Incompressible Fluid Flow. *SIAM J. Sci. Comput.*, **20**, 1165 – 1191, 1999.

[67] Sussmann, M.; Fatemi, E.; Smereka, P.; Osher, S.: An Improved Level Set Method for Incompressible Two-Phase Flows. *Computers and Fluids*, **27**, 663 – 680, 1998.

[68] Sussmann, M.; Smereka, P.; Osher, S.: A Level Set Approach for Computing Solutions to Incompressible Two-Phase Flows. *J. Comput. Phys.*, **114**, 146 – 159, 1994.

[69] Tezduyar, T.E.: Stabilized Finite Element Formulations for Incompressible Flow Computations. In *Advances in Applied Mechanics.* (Hutchinson, J.W.; Wu, T.Y., Eds.), Vol. 28, Academic Press, New York, NY, 1992.

[70] Tezduyar, T.E.; Behr, M.; Liou, J.: A New Strategy for Finite Element Computations Involving Moving Boundaries and Interfaces - The Deforming-Spatial-Domain/Space-Time Procedure: II. Computation of Free-surface Flows, Two-liquid Flows, and Flows with Drifting Cylinders. *Comp. Methods Appl. Mech. Engrg.*, **94**, 353 – 371, 1992.

[71] Tornberg, A.-K.: *Interface Tracking Methods with Application to Multiphase Flows.* Phd thesis, Royal Institute of Technology, 2000.

[72] Unverdi, S.O.; Tryggvason, G.: A Front-Tracking Method for Viscous, Incompressible, Multi-Fluid Flows. *J. Comput. Phys.*, **100**, 25–37, 1992.

[73] Ventura, G.; Budyn, E.; Belytschko, T.: Vector level sets for description of propagating cracks in finite elements. *Internat. J. Numer. Methods Engrg.*, **58**, 1571–1592, 2003.

[74] Ventura, G.; Moran, B.; Belytschko, T.: Dislocations by partition of unity. *Internat. J. Numer. Methods Engrg.*, **62**, 1463–1487, 2005.

[75] Wagner, G.J.; Ghosal, S.; Liu, W.K.: Particle flow simulations using lubrication theory solution enrichment. *Internat. J. Numer. Methods Engrg.*, **56**, 1261 – 1289, 2003.

[76] Wagner, G.J.; Moës, N.; Liu, W.K.; Belytschko, T.: The extended finite element method for rigid particles in Stokes flow. *Internat. J. Numer. Methods Engrg.*, **51**, 293 – 313, 2001.

[77] Wheeler, M.: An elliptic collocation-finite element method with interior penalties. *SIAM J. Numer. Anal.*, **15**, 152–161, 1978.

[78] Y.C. Chang, B. Merriman, T.Y. Hou; Osher, S.: A level set formulation of Eulerian interface capturing methods for incompressible fluid flows. *J. Comput. Phys.*, **124**, 449 – 464, 1996.

[79] Zi, G.; Belytschko, T.: New Crack-Tip Elements for XFEM and Applications to Cohesive Cracks. *Internat. J. Numer. Methods Engrg.*, **57**, 2221 – 2240, 2003.